

# Marine Carbohydrates in Arctic Aerosol Particles and Fog – Diversity of Oceanic Sources and Atmospheric Transformations

Sebastian Zeppenfeld<sup>1</sup>, Manuela van Pinxteren<sup>1</sup>, Markus Hartmann<sup>2</sup>, Moritz Zeising<sup>3</sup>, Astrid Bracher<sup>3,4</sup>, and Hartmut Herrmann<sup>1</sup>

<sup>1</sup> Atmospheric Chemistry Department (ACD), Leibniz-Institute for Tropospheric Research (TROPOS), Leipzig, Germany

<sup>2</sup> Atmospheric Microphysics (AMP), Leibniz-Institute for Tropospheric Research (TROPOS), Leipzig, Germany

<sup>3</sup> Alfred-Wegener-Institute Helmholtz Centre for Polar and Marine Research, Bremerhaven, Germany

<sup>4</sup> Institute of Environmental Physics, University of Bremen, Bremen, Germany

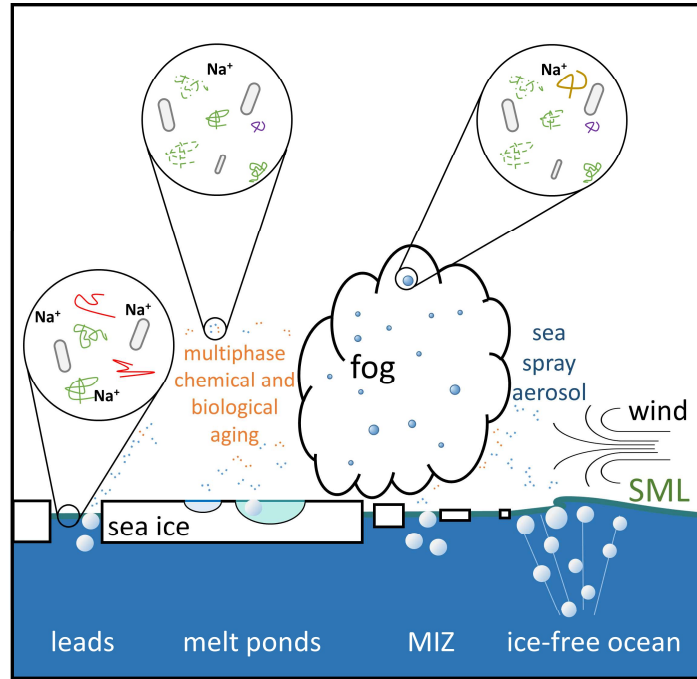
\*Correspondence to: Hartmut Herrmann (herrmann@tropos.de)

Submitted to Atmospheric Chemistry and Physics 2023

## Abstract

Carbohydrates, originating from marine microorganisms, enter the atmosphere as part of sea spray aerosol (SSA) and can influence fog and cloud microphysics as cloud condensation nuclei (CCN) or ice nucleating particles (INP). Particularly in the remote Arctic region, significant knowledge gaps persist about the sources, the sea-to-air transfer mechanisms, atmospheric concentrations, and processing of this substantial organic group. In this ship-based field study conducted from May to July 2017 in the Fram Strait, Barents Sea, and central Arctic Ocean, we investigated the sea-to-air transfer of marine combined carbohydrates (CCHO) from concerted measurements of the bulk seawater, the sea surface microlayer (SML), aerosol particles and fog. Our results reveal a wide range of CCHO concentrations in seawater (22–1070  $\mu\text{g L}^{-1}$ ), with notable variations among different sea-ice-related sea surface compartments. Enrichment factors in the sea surface microlayer (SML) relative to bulk water exhibited variability in both dissolved (0.4–16) and particulate (0.4–49) phases, with the highest values in the marginal ice zone (MIZ) and aged melt ponds. In the atmosphere, CCHO was detected in super- and submicron aerosol particles ( $\text{CCHO}_{\text{aer,super}}$ : 0.07–2.1  $\text{ng m}^{-3}$ ;  $\text{CCHO}_{\text{aer,sub}}$ : 0.26–4.4  $\text{ng m}^{-3}$ ) and fog water ( $\text{CCHO}_{\text{fog,liquid}}$ : 18–22000  $\mu\text{g L}^{-1}$ ;  $\text{CCHO}_{\text{fog,atmos}}$ : 3–4300  $\text{ng m}^{-3}$ ). Enrichment factors for sea-air transfer varied based on assumed oceanic emission sources. Furthermore, we observed rapid atmospheric aging of CCHO, indicating both biological/enzymatic processes and abiotic degradation. This study

- 35 highlights the diverse marine emission sources in the Arctic Ocean and the atmospheric processes
- 36 shaping the chemical composition of aerosol particles and fog.



TOC Figure

37

## 38 1. Introduction

39 Sea spray aerosol (SSA) represents one of the major aerosol species in the lower troposphere over the  
40 remote Arctic Ocean, particularly during the spring and summer months in the Northern Hemisphere  
41 (Chi et al., 2015; Hara et al., 2003; Kirpes et al., 2018; May et al., 2016). Depending on the size  
42 distribution and chemical composition, SSA particles strongly contribute to the populations of cloud  
43 condensation nuclei (CCN) and ice nucleating particles (INP) affecting the polar radiative budget  
44 through the formation of liquid droplets and ice crystals in fog and clouds (DeMott et al., 2016; Lawler  
45 et al., 2021; McCluskey et al., 2018; Penner et al., 2001; Schiffer et al., 2018; Wilbourn et al., 2020).  
46 Notably in the Arctic, one of the regions most affected by global warming, there is still a lack of  
47 knowledge about the relationship between the formation and evolution of clouds and specific  
48 chemical properties of SSA particles (Wendisch et al., 2023).

49 SSA is emitted directly from the ocean surface through wind-driven processes and, as a consequence,  
50 contains the salts and the organic matter (OM) present in seawater, including carbohydrates (CHO) as  
51 one of the largest identified organic fractions (Quinn et al., 2015 and references therein). In  
52 microalgae, bacteria and also more complex marine organisms (e.g. kelp, krill), carbohydrates have  
53 important metabolic, structural and protective functions or are released in response to environmental  
54 stress, such as freezing or lack of nutrients (Krembs et al., 2002; Krembs and Deming, 2008; McCarthy  
55 et al., 1996; Mühlenbruch et al., 2018; Suzuki and Suzuki, 2013; Wietz et al., 2015). In seawater, most  
56 carbohydrates appear as linear or branched oligo- and polysaccharides, commonly referred to as  
57 combined carbohydrates (CCHO). They can be found in both dissolved (*d*CCHO) and particulate  
58 (*p*CCHO) phases, distinguished operationally by a 0.2  $\mu\text{m}$  filtration. These macromolecules consist of  
59 several monosaccharides, such as hexoses, pentoses, deoxy sugars, amino sugars, uronic acids and  
60 amino sugar acids, which are connected via glycosidic bonds (Benner and Kaiser, 2003; Engel and  
61 Händel, 2011; Panagiotopoulos and Sempéré, 2005). Most CCHO are quite stable within the marine  
62 environment unless they are either hydrolyzed in the presence of specific enzymes or in a very acidic  
63 setting (Arnosti, 2000; Panagiotopoulos and Sempéré, 2005). Heterotrophic bacteria use extracellular  
64 enzymes to selectively degrade CCHO into absorbable shorter molecules leaving a certain part as  
65 recalcitrant, more persistent OM (Alderkamp et al., 2007; Becker et al., 2020; Goldberg et al., 2011;  
66 Wietz et al., 2015). While *p*CCHO is mostly attributed to recent productions by local phytoplankton  
67 indicated by high positive correlations with total chlorophyll *a* (TChl-*a*), *d*CCHO appears to be the result  
68 of more complex metabolic and transformation processes after its release (Becker et al., 2020; Fabiano  
69 et al., 1993; Goldberg et al., 2011; Zeppenfeld et al., 2021a). In contrast, dissolved free carbohydrates  
70 (*d*FCHO), short sugars in their monomer form, are quickly consumed by marine microorganisms

71 resulting in much lower concentrations of *d*FCHO compared to CCHO in ambient seawater (Engbrodt,  
72 2001; Engel and Händel, 2011; Ittekkot et al., 1981; Zeppenfeld et al., 2020).

73 In the remote marine atmosphere, carbohydrates are suggested to significantly impact cloud  
74 properties by contributing to both the CCN and INP populations (Alpert et al. 2022; Leck et al., 2013;  
75 Orellana et al., 2011; van Pinxteren et al., 2022). Carbohydrates appear both in super- and submicron  
76 SSA particles (Aller et al., 2017; Leck et al., 2013; Russell et al., 2010; Zeppenfeld et al., 2021a), most  
77 likely resulting from their emission from the surface of the ocean after bubble bursting as part of jet  
78 and film droplets (Veron, 2015; Wang et al., 2017). In addition to the bulk surface seawater, the sea  
79 surface microlayer (SML) as the uppermost layer of the oceanic water column is an important source  
80 of OM, and thus marine carbohydrates, in the SSA. The SML is described as a gelatinous film on top of  
81 the ocean, which is often enriched in surface-active substances or buoyant gel particles compared to  
82 the underlying bulk water (Engel et al., 2017; Wurl et al., 2009, 2011; Zäncker et al., 2017). Entrained  
83 air bubbles rise within the upper part of the water column collecting surface-active organics on the  
84 bubble surfaces from the bulk seawater (Burrows et al., 2014). Eventually they pass the thin SML and  
85 burst there releasing film and jet droplets containing a mixture of substances found within the bulk  
86 water and the SML (Burrows et al., 2014). At the same time, surfactants, exopolymers and microgels  
87 in the SML increase the stability of the cap films of the bubbles, extend their lifetimes and enable the  
88 drainage of water-soluble compounds (Bigg and Leck, 2008; Bikerman, 2013; Sellegri et al., 2006).  
89 Consequently, the sea-air transfer occurs in a chemo-selective manner leading to a strong size-  
90 dependent enrichment of surface-active organics relative to water-soluble sodium (Na<sup>+</sup>) and, hence, a  
91 relative chemical composition of SSA different to the surface seawater (Facchini et al., 2008; O'Dowd  
92 et al., 2004; van Pinxteren et al., 2017; Prather et al., 2013; Quinn et al., 2015; Triesch et al., 2021a, b).  
93 These chemo-selective enrichments of organic substances in the SSA relative to bulk water, especially  
94 in the submicron size range, usually exceed the enrichments in the SML by orders of magnitude (van  
95 Pinxteren et al., 2017; Schmitt-Kopplin et al., 2012). The underlying mechanisms for the chemo-  
96 selective sea-air transfer of carbohydrates, including co-adsorption, are complex and subject of several  
97 recent and ongoing laboratory tank and modelling studies (Burrows et al., 2016; Hasenecz et al., 2020;  
98 Schill et al., 2018; Xu et al., 2023). After their emission, fresh SSA particles, including the contained  
99 carbohydrates, undergo atmospheric aging due to a not yet well-understood interplay of several  
100 atmospheric processes, such as atmospheric acidification, abiotic radical chemistry and biological and  
101 enzymatic modifications (Angle et al., 2021; Hasenecz et al., 2020; Malfatti et al., 2019; Trueblood et  
102 al., 2019; Zeppenfeld et al., 2021a), potentially also altering their microphysical properties.

103 Besides SSA, high concentrations of marine carbohydrates in fog and low-level clouds in the marine  
104 environment are plausible due to the high hygroscopicity of SSA serving as good CCN (Xu et al., 2022)

105 transferring OM from the particle into the liquid phase, the high water-solubility of carbohydrates, and  
106 cloud-borne microorganisms potentially forming carbohydrates in-situ (Matulová et al., 2014). Only a  
107 few studies conducted at field sites exposed to marine air masses measured certain subgroups of  
108 carbohydrates, such as primary saccharides (Dominutti et al., 2022) or transparent exopolymer  
109 particles (TEP) (Orellana et al., 2011; van Pinxteren et al., 2022) so far in fog/clouds. However, the  
110 sources of marine carbohydrates in marine ambient fog/clouds, including  $dFCHO_{fog}$  and  $CCHO_{fog}$ , and  
111 their relationship to the bulk seawater, SML and aerosol particles still lack elucidation.

112 During the summer months, the chemical compounds of natural SSA and marine fog can be studied in  
113 the Arctic Ocean due to the low influence of long-range transported anthropogenic pollution (Bozem  
114 et al., 2019; Schmale et al., 2021). However, the presence and seasonal evolution of Arctic sea ice  
115 divides this pristine region into a complex ensemble of several sea-ice-related sea surface  
116 compartments. These encompass the open leads - sea ice fractures with variable widths ranging from  
117 several to hundreds of meters - and polynyas, which are larger, more persistent areas of open water  
118 within the pack ice. Furthermore, there is the ice-free ocean, the marginal ice zone (MIZ) defined by a  
119 sea ice concentration threshold between 15 and 80% (Rolph et al., 2020), and melt ponds forming and  
120 developing during the melting season on top of the ice floes. These environments are characterized by  
121 different chemical, physical and biological characteristics potentially influencing the quantity and  
122 properties of the SSA emitted. Recent studies observed, for instance, that the number and efficiency  
123 of Arctic INP are strongly dominated by the type of sea-ice-related sea surface compartments that the  
124 air masses had passed before sampling (Creamean et al., 2022; Hartmann et al., 2021;  
125 Papakonstantinou-Presvelou et al., 2022; Porter et al., 2022). However, the individual conclusions still  
126 appear controversial and might be biased by seasonal and interannual variabilities. Consequently,  
127 more systematic studies in the Arctic, also with regard to the chemical properties of the aerosol  
128 particles, are required to achieve more conclusive results.

129 To increase the knowledge about marine carbohydrates as important constituents of SSA and potential  
130 CCN and INP, we present here the results of a comprehensive field study conducted onboard the  
131 German icebreaker RV *Polarstern* from May to July 2017. We performed concerted measurements of  
132 bulk seawater, SML, size-resolved aerosol particles and fog water at different locations dominated by  
133 different sea-ice-related sea surface compartments (ice-free, leads/polynyas, MIZ, melt ponds) in the  
134 Arctic Ocean. All marine and atmospheric compartments are discussed and compared on absolute  
135 CCHO concentrations, calculated  $CCHO/Na^+$  ratios, the relative monosaccharide contribution to CCHO  
136 and the occurrence of  $dFCHO$ . The complex nature of these primary emission mechanisms and  
137 subsequent atmospheric aging of marine CCHO in the Arctic Ocean are discussed in relation to our  
138 findings. Our Arctic results are collated with those from the Southern Ocean at the Antarctic peninsula

139 during the austral summer, as presented in Zeppenfeld et al. (2021a) following a similar experimental  
140 design. While both polar locations are remote marine regions with comparable meteorological  
141 conditions during the sampling periods, the presence of Arctic sea ice adds another dimension of  
142 complexity to data interpretation.

## 143 2. Experimental

### 144 2.1 Study area and field sampling

145 Field samples were gathered during the PS106 (PASCAL/SiPCA) campaign (Macke and Flores, 2018;  
146 Wendisch et al., 2018) conducted from May to July 2017 on board the German icebreaker RV  
147 *Polarstern* in the Fram Strait, Barents Sea and central Arctic Ocean, including a period operating from  
148 a drifting ice station (03–16 June 2017).

149 Marine SML and corresponding bulk water samples were collected from various locations as shown in  
150 **Figure SI 1**. These include the ice-free ocean (four sampling events), open water areas within the pack  
151 ice (20 sampling events, without distinguishing between open leads and polynyas), the MIZ (five  
152 sampling events), and young and aged melt ponds (six sampling events). Using visual characteristics,  
153 melt ponds were categorized as young (small, bluish, clear) or aged (larger, darker blue to greenish,  
154 and turbid with particulates and microalgae). To minimize contamination from exhausts and  
155 wastewater, water samples were taken at distances greater than 100 m from the ship. Seawater was  
156 collected either using a rubber boat or directly from the ice edge. SML samples were obtained by  
157 immersing a glass plate (length: 50 cm, width: 20 cm, thickness: 0.5 cm, sampling area: 2000 cm<sup>2</sup>)  
158 vertically into the surface water and slowly withdrawing it at a speed of approximately 15 cm s<sup>-1</sup> (van  
159 Pinxteren et al., 2012; Zeppenfeld et al., 2021a). The adhered SML film was drawn off the glass plate  
160 surface into a prewashed wide-neck plastic bottle by a framed Teflon wiper. The average thickness of  
161 the SML collected during this field study was 76±10 µm, which was calculated based on the volume of  
162 the SML sample collected, the area of the immersed glass plate and the number of dips as described  
163 by Cunliffe and Wurl (2014). Despite air temperatures during PS106 (median: -0.5°C; minimum: -7.6°C)  
164 hovering around or slightly below the freezing point of seawater, the SML remained unfrozen on the  
165 glass plate during sampling. The corresponding bulk water was taken from a defined depth of 1 m into  
166 LDPE bottles attached to a telescopic rod, except in the bottom closed melt ponds where it was  
167 scooped from the bottom at approximately 20–40 cm depth. Whenever melt pond sampling took  
168 place, snow samples were collected from the ice floe surface roughly 10 m away from the melt pond.  
169 Before each sampling, the sampling containers were first rinsed with a few milliliters of the  
170 corresponding aqueous sample which was disposed immediately after. On board, small aliquots of the  
171 water samples were analyzed immediately for salinity using a conductivity meter (pH/Cond 3320,  
172 WTW), colored dissolved organic matter (CDOM) and particulate absorption (PAB), with more details  
173 in section 2.6. For later chemical analyses (inorganic ions, pH, carbohydrates) 500–1000 mL of 0.2 µm  
174 filtered water sample (dissolved fraction), 0.2 µm polycarbonate filters (particulate fraction) and field  
175 blanks were stored at -20°C.

176 The sampling of ambient aerosol particles was conducted at the starboard side of RV *Polarstern* at the  
177 top of the observation deck at a height of approx. 25 m above sea level as already described in Kecorius  
178 et al. (2019). Size-segregated aerosol particles were sampled in five size ranges (stage 1: 0.05–0.14  $\mu\text{m}$ ,  
179 stage 2: 0.14–0.42  $\mu\text{m}$ , stage 3: 0.42–1.2  $\mu\text{m}$ , stage 4: 1.2–3.5  $\mu\text{m}$ , stage 5: 3.5–10  $\mu\text{m}$  aerodynamic  
180 particle diameter with a 50% cut-off) on aluminum foils by using two synchronized low-pressure Berner  
181 impactors (Hauke, Austria) with a flow rate of 75 L min<sup>-1</sup> and a sampling time of three to six days. To  
182 avoid the condensation of atmospheric water and subsequent microbial activities on the aluminum  
183 foils, a 3 m long heated tubes between the isokinetic inlets and the impactors reduced the relative  
184 humidity of the sampled air to 75-80%, when the ambient relative humidity was higher. During this  
185 field study, the difference of the temperatures of the ambient air at the inlet and the sampled air after  
186 the heating never exceeded 9 K. Consequently, losses of semi-volatile compounds or changes by heat-  
187 induced chemical reactions are expected to be neglectable. Furthermore, the Berner impactors were  
188 thermally insulated by a polystyrene shell. After sampling, the foils were stored in aluminum containers  
189 at -20°C until analysis. In this study, the results from stages 1-3, 4-5 and 1-5 were summed up as  
190 submicron (sub), supermicron (super) and PM<sub>10</sub>, respectively. Details about the size-resolved aerosol  
191 particle samples and corresponding meteorological information are given in (Table SI 1, in total 15  
192 complete sets of Berner foils).

193 Close to the aerosol sampling, fog was collected using the Caltech Active Strand Cloud Collector Version  
194 2 (CASCC2) as described by Demoz et al. (1996). Bulk fog droplets were impacted on Teflon strands  
195 with a diameter of 508  $\mu\text{m}$  and collected into a prewashed Nalgene polyethylene bottle. The flow rate  
196 was 5.3 m<sup>3</sup> min and the 50% lower cut-off was determined to be approximately 3.5  $\mu\text{m}$ . Further  
197 information about the 22 fog samples collected during the PS106 campaign including meteorological  
198 information can be found in Table SI 2 and in Hartmann et al. (2021).

## 199 **2.2 Total aerosol particle mass concentrations**

200 Before and after sampling, the aluminum foils were equilibrated (three days, 20°C, 50% relative  
201 humidity) and weighed using a precise microbalance (Mettler Toledo XP2U, weighing error:  $\pm 4.6 \mu\text{g}$ ).  
202 Total particle mass concentrations ( $\text{mass}_{\text{aer, stage } y}$ ) were calculated for each Berner stage as the ratio  
203 between the difference of the absolute foil masses after and before sampling and the sampled air  
204 volume. Afterwards, aluminum foils were divided for further chemical analyses.

## 205 **2.3 OC/EC in aerosol samples**

206 Organic carbon (OC<sub>aer</sub>) and elemental carbon on Berner aerosol foils were determined as described by  
207 Müller et al. (2010) using a two-step thermographic method (C/S MAX, Seifert Laborgeräte, Germany)  
208 with a nondispersive infrared sensor.



## 209 2.4 Carbohydrates in aerosol particles, fog, snow, seawater and melt ponds

210 Marine carbohydrates in the particulate ( $pCCHO$ ,  $>0.2 \mu\text{m}$ ) and dissolved ( $dCCHO/dFCHO$ ,  $<0.2 \mu\text{m}$ )  
211 phases, including truly dissolved molecules and small colloids, were quantified from seawater and melt  
212 pond samples following the protocol presented by Zeppenfeld et al. (2020, 2021a) using high-  
213 performance anion-exchange chromatography with pulsed amperometric detection (HPAEC-PAD)  
214 equipped with a Dionex CarboPac PA20 analytical column (3 mm  $\times$  150 mm) and a Dionex CarboPac  
215 PA20 guard column (3 mm  $\times$  30 mm). The monosaccharides fucose (Fuc), rhamnose (Rha), arabinose  
216 (Ara), galactose (Gal), glucose (Glc), xylose (Xyl), mannose (Man), fructose (Fru), galactosamine (GalN),  
217 glucosamine (GlcN), muramic acid (MurAc), galacturonic acid (GalAc), and glucuronic acid (GlcAc) were  
218 identified by their retention times.  $dFCHO$  represent the sum of identifiable monosaccharides before,  
219 and  $dCCHO$  and  $pCCHO$  additionally released after an acid hydrolysis (0.8 M HCl, 100°C, 20 h).  $CCHO$  is  
220 the sum of  $dCCHO$  and  $pCCHO$ .  $CHO$  represents the sum of  $CCHO$  and  $dFCHO$ , and consequently  
221 encompasses all carbohydrates measured within this study. **Figure 1** gives an overview of the here  
222 used carbohydrate-related abbreviations. Marine carbohydrates in fog water, snow and extracts from  
223 size-resolved aerosol particles were measured with ( $CCHO_{\text{fog}}$ ,  $CCHO_{\text{aer}}$ ) or without ( $dFCHO_{\text{fog}}$ ,  $dFCHO_{\text{aer}}$ )  
224 prior acid hydrolysis.

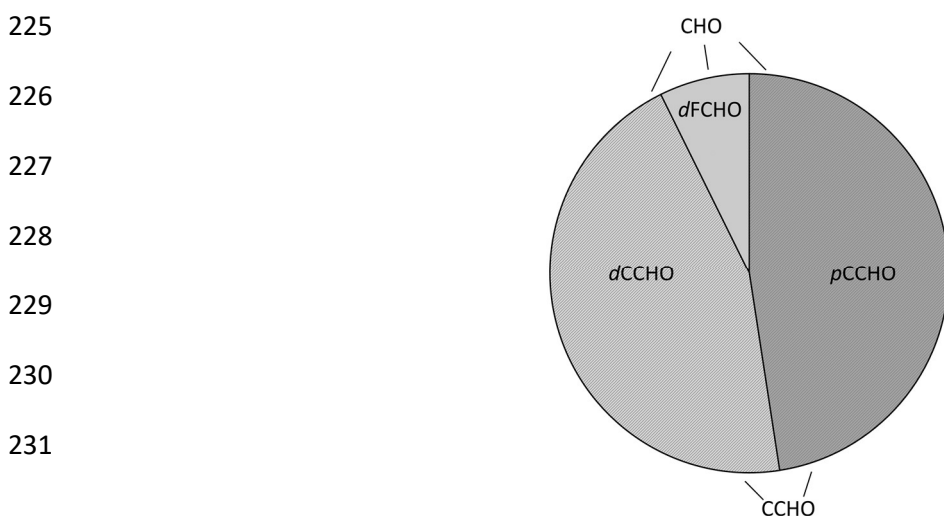


**Figure 1.** Overview of the abbreviations for carbohydrates ( $CHO$ ) in seawater.  $CCHO$ : combined carbohydrates;  $pCCHO$ : particulate combined carbohydrates,  $dCCHO$ : dissolved combined carbohydrates;  $dFCHO$ : dissolved free carbohydrates.

## 232 2.5 Sodium and pH in aerosol particles, fog, seawater and melt ponds

233 Major inorganic ions, including sodium ( $\text{Na}^+$ ), were determined from 0.45  $\mu\text{m}$  filtered aqueous extracts  
234 of the size-resolved aerosol samples (50% of the Berner foil in 2 mL ultrapure water), fog water, diluted  
235 (1:15 000) seawater and melt pond samples using ion chromatography (ICS-3000, Dionex) as described  
236 by Müller et al. (2010). In this study, we discuss the results for  $\text{Na}^+$  as a proxy for SSA emissions in  
237 remote marine regions. Additionally, the pH was monitored by an additional autosampler sample

238 conductivity and pH accessory (Dionex) in all seawater, melt pond and, whenever enough sample  
239 volume was available, in fog water.

## 240 **2.6 Absorption by phytoplankton, non-algal particles and colored dissolved** 241 **organic matter in seawater and melt pond samples**

242 For the investigation of bio-optical parameters in seawater and melt pond samples, the particulate  
243 fraction was collected by filtering the water samples (5–500 mL) onto glass-fiber filters (GF/F,  
244 Whatman), while the dissolved fraction was filtered through 0.2  $\mu\text{m}$  Spartan syringe filters (Whatman,  
245 Germany) immediately after sampling. The GF/F filters were analyzed to determine the absorption  
246 spectra (i.e. 320–844 nm, 2 nm resolution) using the quantitative filtration technique with an  
247 integrative-cavity absorption meter setup (QFT-ICAM) as developed by Röttgers et al. (2016). We  
248 followed the protocol by Liu et al. (2018) for the instrument used here and the determination of the  
249 absorption coefficients by total particles ( $a_{p440}$ ), phytoplankton ( $a_{ph440}$ ) and non-algal particles  
250 ( $a_{NAP440}$ ) at  $\lambda=440$  nm.

251 The absorption for the dissolved fraction ( $a_{CDOM}(\lambda)$ ) between 270 and 750 nm (1 nm resolution) were  
252 measured as triplicates using a long path length liquid waveguide capillary cell (LWCC) system following  
253 the procedure by Lefering et al. (2017) and including the correction for salinity effects by Röttgers et  
254 al. (2014) as described for our instrumentation in Álvarez et al. (2022). The absorption coefficients in  
255 the visible at 443 nm ( $a_{CDOM443}$ ) and UV at 350 nm ( $a_{CDOM350}$ ) bands were used as indicators of CDOM  
256 magnitude.

## 257 **2.7 Supporting observations**

258 The German research vessel *Polarstern* performs continuous meteorological surface measurements  
259 during times of ship operation. For this study, we used the data from the HMP155  
260 thermometer/hygrometer probe (Vaisala), the ultrasonic anemometer (Thies Clima) and the FS11  
261 visibility sensor (Vaisala) installed at a height of 29 m, 39 m and 20 m above sea level, respectively. The  
262 quality-controlled data made available by the operators on the public repository PANGAEA  
263 (Schmithüsen, 2018, 2019) supported the interpretation of the results of this study.

264 The 120 h back-trajectories were computed for the sampling periods of the size-resolved aerosol  
265 particles and fog water events using the NOAA HYSPLIT model (Stein et al., 2015). The back-trajectories  
266 were calculated on an hourly basis using the GDAS1 meteorological fields (Global Data Assimilation  
267 System; 1° latitude/longitude; 3-hourly) and at arrival heights of 50, 250 and 1000 m. Sea ice  
268 concentration data were retrieved from ERDDAP (Environmental Research Division's Data Access  
269 Program), a data server maintained by NOAA (National Oceanic and Atmospheric Administration). The  
270 MIZ was defined here as the oceanic region with a sea ice concentration between 15 and 80%. Data

271 on melt pond fractions were accessed from the sea ice remote sensing data achieve of the University  
272 of Bremen (<https://data.seaice.uni-bremen.de>, Istomina (2020)).

## 273 **2.8 Statistics, calculations and visualization**

274 Statistical analyses, calculations and visualization were performed in OriginPro, Microsoft Excel and R  
275 version 4.2.1 using the following packages: oce, ocedata, ncdf4, openair, ggplot2, reshape2, scales,  
276 lubridate, cmocean, maps, mapdata, rgdal, raster, RColorBrewer, sp. Time-resolved back-trajectories  
277 and sea ice maps were combined using R to compute and visualize the air mass history regarding the  
278 sea-ice-related sea surface compartments that have been passed. As a result, relative residence times  
279 of the air masses over certain surface features (ice-free, MIZ, pack ice, land) 12 hours before sampling  
280 were calculated based on defined thresholds for sea ice concentration: less than 15% for ice-free  
281 ocean, 15-80% for MIZ and over 80% for pack ice. Based on the remote sensing data used, we did not  
282 distinguish between open leads and melt ponds as the air traversed the pack ice. Box-whisker plots  
283 represent the interquartile range (box), median (horizontal line within the box), average (open square)  
284 and the minimum and maximum values of the datasets (whiskers). Measured mean values are given  
285 together with the calculated standard deviations ( $\pm$ ). Correlations between two measured variables  
286 were expressed via the Pearson correlation coefficient  $R$ . The thresholds of significance were set for  
287 the p-values 0.1, 0.05, 0.01 and 0.001.

288 Enrichment factors for CCHO in the SML ( $EF_{SML}$ ) relative to the corresponding bulk sample in different  
289 sea-ice-related sea surface compartments (ice-free, leads/polynyas, MIZ, melt ponds) were calculated  
290 based on **Formula 1** with  $[x]_{SML}$  and  $[x]_{bulk}$  representing the concentrations of either  $pCCHO$  or  $dCCHO$ .  
291 For the calculation of enrichment factors of CCHO in aerosol particles on Berner stage  $y$  ( $EF_{aer,stage y}$ ;  
292 **Formula 2**) and fog water ( $EF_{fog}$ ; **Formula 3**) relative to the bulk water samples, the ocean was assumed  
293 as the most likely source of atmospheric  $Na^+$ . For the calculations of  $EF_{aer}$  and  $EF_{fog}$ , we used the median  
294 value of all  $CCHO_{bulk} / Na^+_{bulk}$  ratios found in the samples of a certain sea-ice-related sea surface  
295 compartment (ice-free, leads/polynyas, MIZ, melt ponds) over the whole campaign.

296

$$297 \quad EF_{SML} = \frac{[x]_{SML}}{[x]_{bulk}} \quad (1)$$

$$298 \quad EF_{aer,stage y} = \frac{[x]_{aer,stage y} / [Na^+]_{aer,stage y}}{[x]_{bulk} / [Na^+]_{bulk}} \quad (2)$$

$$299 \quad EF_{fog} = \frac{[x]_{fog} / [Na^+]_{fog}}{[x]_{bulk} / [Na^+]_{bulk}} \quad (3)$$

### 300 **3. Results and Discussion**

301 The sources of SSA particles, and hence of atmospheric marine carbohydrates, microbial cells and  
302 fragments, in the Arctic are diverse and influenced by the prevailing sea ice conditions. Here, we  
303 present the concentrations and relative compositions of CCHO in the SML and bulk water from the ice-  
304 free ocean, open leads and polynyas within the pack ice, melt ponds and the MIZ. After this, the  
305 different sea-ice-related sea surface compartments are linked with the atmospheric CCHO found in  
306 ambient size-resolved aerosol particles and fog water. The influences of the air mass history,  
307 enrichments of CCHO towards  $\text{Na}^+$  during the sea-air transfer and secondary atmospheric  
308 transformations processes altering atmospheric CCHO are discussed.

#### 309 **3.1 Sea ice influences the properties of the sea surface water**

310 **Variable CCHO concentrations in the Arctic surface water.** CCHO were found in the dissolved ( $d\text{CCHO}$ )  
311 and particulate ( $p\text{CCHO}$ ) phases of the SML and bulk water samples collected from the ocean and the  
312 melt ponds during the PS106 campaign. Among all aqueous samples, regardless of the sampling  
313 environment and depth (SML versus bulk),  $d\text{CCHO}$  ( $13\text{--}640 \mu\text{g L}^{-1}$ ;  $\text{mean}_{d\text{CCHO}} = 82 \pm 110 \mu\text{g L}^{-1}$ ;  $n=70$ )  
314 and  $p\text{CCHO}$  ( $4\text{--}810 \mu\text{g L}^{-1}$ ;  $\text{mean}_{p\text{CCHO}} = 84 \pm 160 \mu\text{g L}^{-1}$ ;  $n=70$ ) concentrations were highly variable.  
315 However, the minimum, maximum and mean values of both  $d\text{CCHO}$  and  $p\text{CCHO}$  ranged within the  
316 same orders of magnitude. CCHO as the sum of  $d\text{CCHO}$  and  $p\text{CCHO}$  ranged between  $22\text{--}1070 \mu\text{g L}^{-1}$   
317 ( $\text{mean}_{\text{CCHO}} = 166 \pm 250 \mu\text{g L}^{-1}$ ;  $n=70$ ).

318 Large differences in the mean values and standard deviations of CCHO were observed among the four  
319 sea-ice-related sea surface compartments in the Arctic (leads/polynyas within the pack ice, MIZ, ice-  
320 free ocean, melt ponds) as shown in **Figure 2a+b**. The highest mean values for  $d\text{CCHO}$  and  $p\text{CCHO}$  were  
321 observed in the SML of the MIZ ( $\text{mean}_{d\text{CCHO}, \text{SML}, \text{MIZ}} = 190 \pm 160 \mu\text{g L}^{-1}$ ;  $\text{mean}_{p\text{CCHO}, \text{SML}, \text{MIZ}} = 370 \pm 310 \mu\text{g L}^{-1}$ ;  
322  $n=5$ ) and melt ponds ( $\text{mean}_{d\text{CCHO}, \text{SML}, \text{melt ponds}} = 190 \pm 240 \mu\text{g L}^{-1}$ ;  $\text{mean}_{p\text{CCHO}, \text{SML}, \text{melt ponds}} = 200 \pm 310 \mu\text{g L}^{-1}$ ;  
323  $n=6$ ), while the SML of the lead/polynya ( $\text{mean}_{d\text{CCHO}, \text{SML}, \text{lead/polynya}} = 70 \pm 75 \mu\text{g L}^{-1}$ ;  
324  $\text{mean}_{p\text{CCHO}, \text{SML}, \text{lead/polynya}} = 70 \pm 120 \mu\text{g L}^{-1}$ ;  $n=20$ ) and ice-free open ocean ( $\text{mean}_{d\text{CCHO}, \text{SML}, \text{ice-}}$   
325  $\text{free}} = 73 \pm 12 \mu\text{g L}^{-1}$ ;  $\text{mean}_{p\text{CCHO}, \text{SML}, \text{ice-free}} = 36 \pm 5 \mu\text{g L}^{-1}$ ;  $n=4$ ) samples tended to contain less CCHO. CCHO  
326 concentrations exhibited significant variability among the melt ponds, with higher concentrations  
327 observed in aged ponds (depths ranging from 40 cm to open-bottomed) compared to younger ones,  
328 where depths varied between 20 and 40 cm.

329 The lower SML concentrations from this study for the Arctic ice-free open ocean and lead/polynya  
330 samples align closely with several other investigations. Specifically, our results are comparable to Gao  
331 et al. (2012), who studied the SML of Arctic leads ( $\text{mean}_{d\text{CCHO}, \text{SML}, \text{Arctic leads}} = 163 \pm 104 \mu\text{g L}^{-1}$ ;  
332  $\text{mean}_{p\text{CCHO}, \text{SML}, \text{Arctic leads}} = 35 \pm 25 \mu\text{g L}^{-1}$ ;  $n=4$ ), and Zeppenfeld et al. (2021), focusing on the ice-free part

333 of the Southern Ocean west of the Antarctic peninsula during the austral summer  
 334 ( $\text{mean}_{d\text{CCHO, SML, Southern Ocean}} = 48 \pm 63 \mu\text{g L}^{-1}$ ;  $\text{mean}_{p\text{CCHO, SML, Southern Ocean}} = 72 \pm 53 \mu\text{g L}^{-1}$ ;  $n=18$ ). Similarly, our  
 335 data mirror findings from the tropical Cape Verde ( $\text{mean}_{d\text{CCHO, SML, Cape Verde}} = 85 \pm 30 \mu\text{g L}^{-1}$ ; van Pinxteren  
 336 et al., 2023) and the Peruvian upwelling region ( $\text{mean}_{d\text{CCHO, SML, Peru}} \approx 92 \pm 32 \mu\text{g L}^{-1}$ ; Zäncker et al., 2017).  
 337 Consequently, the Arctic MIZ and melt ponds, especially the aged ones with advanced microbiological  
 338 activities, stood out with elevated CCHO within the Arctic and also compared to tropical and other  
 339 polar regions.

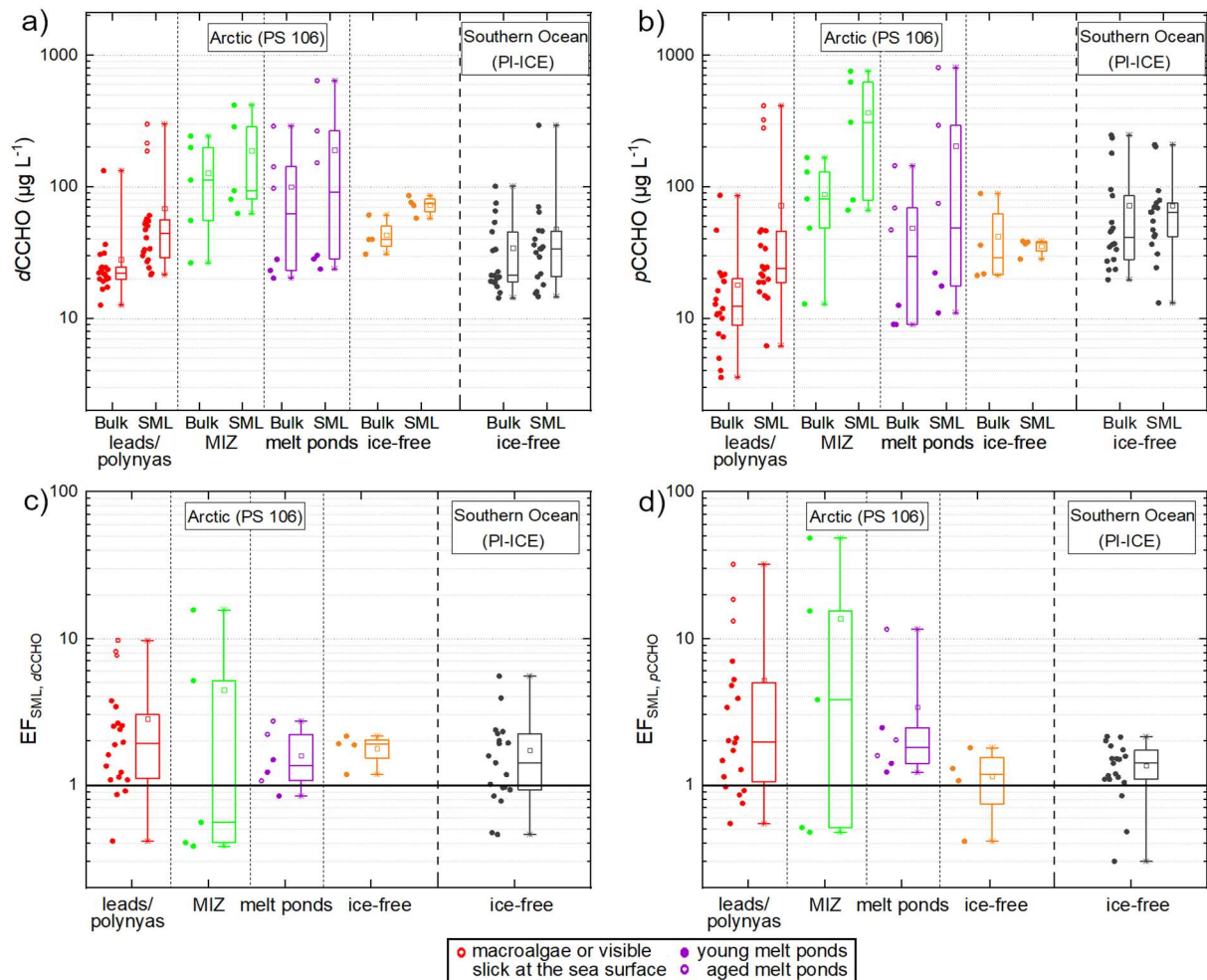


**Figure 2.** Scattered box-whisker plots showing the concentrations of a)  $d\text{CCHO}$  and b)  $p\text{CCHO}$  in the bulk and SML samples from the open leads and polynyas in the pack ice (red), the MIZ (green), ice-free open ocean (orange) and young and aged melt ponds (purple) collected during the PS106 campaign in the Arctic in comparison to the ice-free part of the Southern Ocean west of the Antarctic Peninsula investigated during the PI-ICE campaign in 2019 (black) as published in Zeppenfeld et al. (2021). EFs between SML and bulk water are shown in c) for  $d\text{CCHO}$  and d) for  $p\text{CCHO}$ . The black horizontal line represents an  $\text{EF}=1$  meaning no enrichment or depletion.

340 **Variable enrichments of CCHO in the SML.** The enrichment factors ( $\text{EF}_{\text{SML}}$ ) of the CCHO in the SML  
 341 relative to the corresponding bulk water ranged between 0.4 and 16 for  $d\text{CCHO}$  (Figure 2c), while the  
 342  $\text{EF}_{\text{SML}}$  for  $p\text{CCHO}$  varied between 0.4 and 49 (Figure 2d). 80% of the SML samples were moderately or  
 343 highly enriched in marine carbohydrates with only a few cases of depletion (7 for  $d\text{CCHO}$  and 8 for  
 344  $p\text{CCHO}$  out of 35 in total). With a median  $\text{EF}_{\text{SML}, p\text{CCHO}, \text{MIZ}}$  value of 3.8 and a mean of 13.8, the enrichment

345 of *p*CCHO in the MIZ stood out compared to the *p*CCHO in other sea-ice-related sea surface  
346 compartments and to *d*CCHO overall. However, it should be noted that the number of MIZ samples  
347 was low and median and mean values were dominated by three sample pairs with very high  $EF_{SML}$   
348 values. Low to moderate enrichments for *d*CCHO and *p*CCHO were typically found in the lead/polynya  
349 samples from the pack ice (median  $EF_{SML,dCCHO,leads/polynyas}=1.9$ ; median  $EF_{SML,pCCHO,leads/polynyas}=2.0$ ,  $n=20$ ).  
350 However, three lead samples showed quite high *d*CCHO & *p*CCHO concentrations in the SML compared  
351 to the corresponding bulk samples resulting in high  $EF_{SML,dCCHO,leads/polynyas}$  up to 10 and  
352  $EF_{SML,pCCHO,leads/polynyas}$  up to 32. The exceptionally high EFs of these three samples can be explained by  
353 the observation of slicks - visible films on the sea surface with altered reflectance and typically high  
354 enrichments of organics (Cunliffe et al., 2013; Stolle et al., 2010; Williams et al., 1986; Wurl et al., 2009)  
355 as well as the presence of macroalgae floating at the ocean's surface near the sampling site. Even  
356 though the macroalgae were not collected themselves, their exudates or fragments might have been  
357 released, accumulated and distributed in the SML close-by and thus sampled. Consequently, the few  
358 samples with high EFs in open leads might rather represent exceptional events as spatially small-scale  
359 phenomena.

360 The slight to high enrichments for *d*CCHO and *p*CCHO in this study are in good agreement with the  
361 values reported by Gao et al. (2012), who determined  $EF_{SML,dCCHO}$  between 3.5 and 12, and  $EF_{SML,pCCHO}$   
362 between 1.7 and 7.0 for open leads within the central Arctic Ocean. Furthermore, the  $EF_{SML,dCCHO}$  of the  
363 four Arctic sea-ice-related sea surface compartments reported here were not significantly different  
364 compared to values found in the ice-free part of the Southern Ocean (ANOVA, one-way, 0.05  
365 significance level). For the *p*CCHO, however, the average  $EF_{SML}$  in the Arctic MIZ was significantly higher  
366 than the one of the Southern Ocean, whereas the  $EF_{SML,pCCHO}$  of the ice-free ocean in the Arctic were  
367 similar to the Southern Ocean.

368 For explaining the accumulation in the SML, previous studies proposed several mechanisms and  
369 processes, which fundamentally differ for the dissolved and particulate carbohydrates. The enrichment  
370 of *p*CCHO in the SML might be dominated by an interplay of density-related and wind-driven processes.  
371 For instance, the positive buoyancy of TEP, a subgroup of *p*CCHO, leads to an upward flux serving as a  
372 continual vehicle for marine organisms and attached chemical compounds (Azetsu-Scott and Passow,  
373 2004; Mari et al., 2017). Furthermore, strong winds can cause a short-term mixing of the upper water  
374 column reducing the  $EF_{SML}$  of particulates (Obernosterer et al., 2008) or TEP (Wurl et al., 2009; Zäncker  
375 et al., 2021), while the wind-induced entrainment of air and the bubbling of seawater convert dissolved  
376 negatively charged *d*CCHO and colloids into larger aggregates due to their sticky properties leading to  
377 an enrichment of *p*CCHO in the SML (Passow, 2002; Robinson et al., 2019; Wurl et al., 2011). The  
378 enrichment of *d*CCHO and also *d*FCHO in the SML is attributed to co-adsorption to other surface-active

379 compounds from the seawater matrix being scavenged at the surface of rising bubbles (Burrows et al.,  
380 2016; Hasenecz et al., 2020; Schill et al., 2018; Xu et al., 2023). Additionally, microbial processes in the  
381 SML could enhance the enrichment through in-situ *d*CCHO production by micro- or macroalgae, while  
382 photolysis and enzymatic degradation of *d*CCHO into *d*FCHO by heterotrophic bacteria could decrease  
383 the SML enrichment. Specific to the Arctic, the release of meltwater from the sea ice could be an  
384 additional source for carbohydrates in the SML, considering the production of CCHO, exopolymeric  
385 substances (EPS) and TEP by sea ice algae and bacteria as a protection strategy against freezing damage  
386 and fluctuating salinity in sea ice (Aslam et al., 2016; Krembs et al., 2002; Krembs and Deming, 2008).  
387 This aligns well with the finding by Galgani et al. (2016) who observed labile, fresh OM in the SML of  
388 melt ponds compared to the rather old, refractory nature of the SML in the surrounding open leads.  
389 Hence, melting of sea ice could explain the extraordinarily high  $EF_{SML}$  observed in some, but not all,  
390 SML samples from the MIZ and melt ponds. In summary, several processes might be responsible for  
391 enrichment processes in the SML, especially in the Arctic, where the melting of sea ice could strongly  
392 bias the physiochemical processes usually observed in controlled tank experiments.

393 ***High and low salinities due to freezing and melting of sea ice.*** While the surface seawater of the Arctic  
394 Ocean is very saline, the Arctic sea ice is much fresher due the separation into salt-free ice crystals and  
395 a salty brine during its formation from seawater and a subsequent salt loss from gravity drainage in  
396 winter and flushing during summer (Notz and Worster, 2009). During the late spring and summer  
397 period of this study, when strong melting of sea ice occurs, a large amount of freshwater enters the  
398 surface of the ocean creating inhomogeneities of salinity within the surface of the ocean. In both the  
399 ice-free ocean and the pack ice, where sea ice exists, but the melting rate is low, salinities of the SML  
400 and the bulk water ranged in this study between 30.9 and 34.5 (Zeppenfeld et al., 2019b), which is  
401 typical for the SML and the surface bulk water of the Arctic Ocean (Vaqué et al., 2021). Within the MIZ,  
402 where freshwater from melting sea ice quickly mixes with the salty ocean water, salinities were similar  
403 with values in this study between 30.1 and 33.4, however, also with an exception in the SML of 25.7.  
404 Melt ponds that were not yet joined at the bottom with the ocean below, were much fresher with  
405 lower and more variable salinities ranging from 4.3 to 19.5 (Zeppenfeld et al., 2019b). With a few  
406 exceptions, salinity discrepancies between the SML and the corresponding bulk water were small in  
407 most cases.

408 Sea-air transfer studies usually refer to open ocean scenarios with high salinities in the seawater and  
409 without the presence of melting sea ice. For the calculation of enrichment factors of organics in aerosol  
410 particles ( $EF_{aer}$ ) or fog ( $EF_{fog}$ ), the concentrations of  $Na^+$  – a major compound of sea salt – in the  
411 seawater bulk is included by default (see equations 2 and 3). However, the Arctic is a more complex  
412 marine environment where salinities, and hence  $Na^+$  concentrations, can vary widely as melting

413 progresses. This may strongly influence the mechanisms behind the bubble bursting process, the  
414 CCHO/Na<sup>+</sup> ratios in the bulk seawater and the SML, and thus also the EF<sub>aer</sub> and EF<sub>fog</sub> as it will be  
415 discussed in section 3.4. Consequently, the variability of salinity in Arctic seawater and melt ponds  
416 should be considered for sea-air transfer studies that rely on Na<sup>+</sup> values.

417 ***Four sea-ice-related sea surface compartments with different characteristics.*** The high Arctic differs  
418 from other oceanic regions in the presence, formation and melting of sea ice creating sea-ice-related  
419 sea surface compartments (ice-free, leads/polynyas, MIZ, melt ponds) with individual biological and  
420 chemical characteristics, such as CCHO concentrations, enrichments in the SML and salinities. This  
421 might potentially impact the transfer of substances from the ocean to the atmosphere, chemo-  
422 selective enrichment processes of marine CCHO in the primary marine aerosol particles and thus their  
423 microphysical properties. The next sections will elucidate if and how these differences within the  
424 individual compartments relate to CCHO<sub>aer</sub> and CCHO<sub>fog</sub>.



## 425 **3.2 Sea spray aerosol and therein contained combined carbohydrates**

426 ***Breaking waves as the main mechanism for SSA emissions is not unambiguous in the Arctic.*** In the  
427 open ocean, the emission flux of SSA and hence its inorganic and organic constituents mainly depend  
428 on the wind speed as the driving force for breaking waves and bubble bursting, and furthermore on  
429 the seawater temperature, salinity, wave properties and organic surface-active substances (Grythe et  
430 al., 2014). In this study, atmospheric sodium ( $\text{Na}^+_{\text{aer,PM10}}$ ), the best tracer for SSA (Barthel et al., 2019),  
431 ranged between 12 and 765  $\text{ng m}^{-3}$  (**Table SI 1**).  $\text{Na}^+_{\text{aer,PM10}}$  showed a good correlation ( $R=0.80$ ,  $p<0.001$ ,  
432 **Figure 3a**) with wind speed, measured at the sampling site and averaged over the sampling time, if all  
433 aerosol samples are included. However, the strength of this correlation decreased sharply ( $R=0.59$ ,  
434  $p<0.1$ ), when only samples collected over the MIZ and the pack ice were included, while the few  
435 samples from the open ocean characterized by high  $\text{Na}^+$  values were excluded. This is due to the  
436 presence of sea ice in the high Arctic, which likely alters and conceals the classical wind-driven  
437 mechanisms of breaking waves and bubble bursting resulting in SSA emission. Firstly, sea ice covers a  
438 significant part of the Arctic Ocean strongly reducing the area releasing SSA. Secondly, the presence of  
439 sea ice causes an attenuation of the high-frequency wind-sea waves, while longer waves, such as  
440 swells, can remain (Thomson, 2022). Consequently, the effect of wind on the SSA emission mechanisms  
441 within the open leads and the MIZ might be different than in the ice-free ocean. For those sea-ice-  
442 dominated compartments, alternative wind-independent sources of ascending bubbles were  
443 suggested, such as melting sea ice nearby, respiration of phytoplankton or sea-air heat exchange below  
444 the sea surface (Chen et al., 2022 and references therein). Thirdly, in contrast to other marine regions  
445 with quite homogeneous ocean salinities, and hence sodium concentrations, the salinities among the  
446 different Arctic sea-ice-related sea surface compartments are more variable due to the melting of sea  
447 ice. Previously, the results of a sea-air transfer tank experiment with artificial seawater showed the  
448 influence of salinity on the relative particle number concentrations of emitted SSA for salinities below  
449 15 – values especially relevant for melt ponds in the Arctic – while changes at higher salinities did not  
450 result in a measurable effect (Zábori et al., 2012). Additionally, organics with potential surface-active  
451 properties are very variable in these disparate Arctic environments, as discussed for CCHO in section  
452 3.1. Organic surfactants can alter the ocean surface's ability to form whitecaps and the lifetime of  
453 bubbles (Bigg and Leck, 2008; Callaghan et al., 2012; Grythe et al., 2014) and therefore SSA properties.  
454 Finally, blowing snow over the sea ice could serve as an additional source of atmospheric  $\text{Na}^+_{\text{aer}}$  when  
455 a certain air-temperature-dependent wind speed threshold is exceeded. (Chen et al., 2022; Gong et  
456 al., 2023; Huang and Jaeglé, 2017; Yang et al., 2008). Consequently, connections and correlations for  
457 the release of SSA particles in the heterogeneous high Arctic are more difficult to explore than other

458 marine environments without sea ice. It can be assumed that this complex setting influences not only  
 459 the release of inorganic constituents from seawater, but also its organic compounds, such as CCHO.

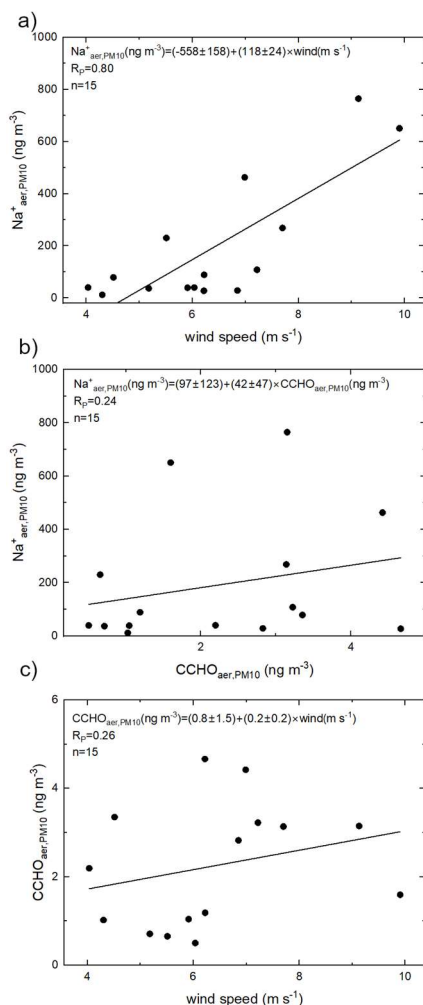
460

461

462

463

464



465

466

467

468

469

470

471

472

473

474 **Figure 3.** Correlations between a)  $\text{Na}^+_{\text{aer,PM10}}$  and the averaged wind speed, b)  $\text{Na}^+_{\text{aer,PM10}}$  and  $\text{CCHO}_{\text{aer,PM10}}$ , c)  $\text{CCHO}_{\text{aer,PM10}}$  and averaged wind speed.

475 ***CCHO<sub>aer</sub> distributed in all size modes.*** During the PS106 campaign, the overall atmospheric  
 476 concentrations of  $\text{CCHO}_{\text{aer,PM10}}$  ranged between 0.5 and 4.7 ng m<sup>-3</sup> (Table SI 1). Combined  
 477 carbohydrates were found on both supermicron ( $\text{CCHO}_{\text{aer,super}} = 0.07\text{--}2.1$  ng m<sup>-3</sup>) and submicron  
 478 particles ( $\text{CCHO}_{\text{aer,sub}} = 0.26\text{--}4.4$  ng m<sup>-3</sup>). Thus, these  $\text{CCHO}_{\text{aer}}$  values ranged within the same orders of  
 479 magnitude as in the Arctic studies by Karl et al. (2019) and Leck et al. (2013) or the study conducted at  
 480 the western Antarctic peninsula by Zeppenfeld et al. (2021a).  $\text{CCHO}_{\text{aer}}$  appeared in all of the five size  
 481 classes in variable concentrations (Figure 4a). Although the average concentrations were similar on all  
 482 stages, local maxima were observed on stages 2 (0.14–0.42 μm) and 5 (1.2–10 μm). A similar size  
 483 distribution of marine  $\text{CCHO}_{\text{aer}}$  in these specific size ranges, but more pronounced, has been already  
 484 observed in the ice-free part of the Southern Ocean by Zeppenfeld et al. (2021a) explaining these  
 485 findings with a likely release of marine polysaccharides from the ocean as part of film and jet droplets.  
 486 Possibly, the aerosol size distribution of marine polysaccharides resulting from wind-driven bubble

487 bursting emissions are not as obvious in this Arctic study as it was in the ice-free Southern Ocean due  
 488 to the presence of Arctic sea ice suppressing and altering the local SSA emission mechanisms as  
 489 indicated in the previous section. The relative contribution of  $CCHO_{aer}$  to  $mass_{aer}$  varied between 0.01%  
 490 and 4% (**Figure 4b**), while the carbon contained within the combined carbohydrates ( $C-CCHO_{aer}$ )  
 491 contributed 0.06 to 4.9% to the  $OC_{aer}$  in the size-resolved aerosol particles (**Figure 4c**). These  
 492 contributions agree well with the findings in marine aerosol particles from the Southern Ocean  
 493 (Zeppenfeld et al., 2021a).

494

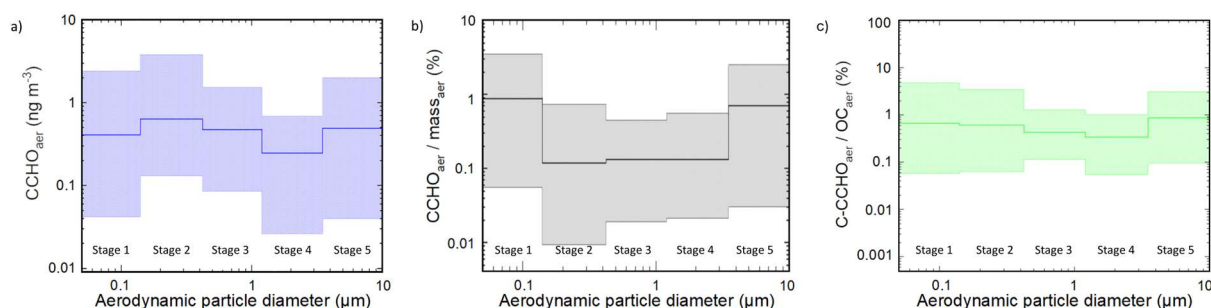


**Figure 4.** a) Concentration of combined carbohydrates in size-resolved aerosol particles ( $CCHO_{aer}$ ), b) ratio of  $CCHO_{aer}$  to the total particle mass concentration ( $mass_{aer}$ ), c) ratios of carbon contained within the combined carbohydrates in aerosol particles ( $C-CCHO_{aer}$ ) to organic carbon in aerosol particles ( $OC_{aer}$ ). The bold lines represent the average concentrations during the PS106 campaign. The hatched areas show the range between the maximum and minimum values. The aerodynamic particle diameter refers to sampling conditions at relative humidity of max. 80%.

495 Unlike the study conducted in the Southern Ocean (Zeppenfeld et al., 2021a),  $CCHO_{aer,PM10}$  in this study  
 496 showed no significant correlations with  $Na^+_{aer,PM10}$  ( $R=0.24$ ,  $p>0.1$ , **Figure 3b**) or wind speed ( $R=0.26$ ,  
 497  $p>0.1$ , **Figure 3c**). The presence of sea ice resulting in melt ponds and MIZ regions, and the interplay of  
 498 multiple emission mechanisms in the Arctic, as discussed earlier, could account for this complexity.  
 499 However, if the correlations are resolved for the different Berner impactor stages (i.e. size ranges), a  
 500 large variability can be observed (**Figure 5**). A higher correlation was found especially on stage 4  
 501 ( $1.2-3.5 \mu m$ ) between  $CCHO_{aer,stage 4}$  and  $Na^+_{aer,stage 4}$  ( $R=0.76$ ,  $p<0.01$ ), while the Pearson correlations  
 502 coefficients for the other Berner stages were much lower. This could indicate the same marine source  
 503 and wind-driven emission mechanism for both chemical constituents in this supermicron aerosol size  
 504 mode, while other aerosol size modes might have been influenced by atmospheric aging and wind-  
 505 independent emission mechanisms as already mentioned for  $Na^+_{aer}$  in the previous section. This  
 506 observation agrees well with the findings by Bigg and Leck (2008) and Leck (2002) reporting submicron  
 507 polymer gel particles, likely consisting of polysaccharides, in the atmosphere of the high Arctic  
 508 containing almost no sea salt and showing large similarities to those particles found in open leads  
 509 close-by. This is quite surprising considering that the mechanism of wind-driven wave breaking is quite  
 510 limited due to the lack of long fetches of open water (Held et al., 2011; Norris et al., 2011).

511  
512  
513  
514  
515  
516  
517  
518

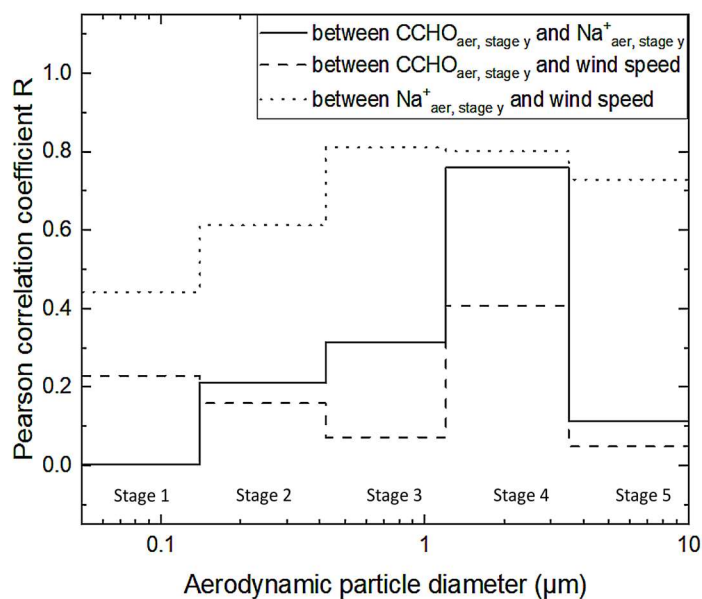


**Figure 5.** Pearson correlation coefficient R between CCHO<sub>aer,stage y</sub> and Na<sup>+</sup><sub>aer,stage y</sub> (solid line), between CCHO<sub>aer,stage y</sub> and the average wind speed (dashed line), and between Na<sup>+</sup><sub>aer,stage y</sub> and the average wind speed (dotted line) for each stage y of the Berner impactor.

519 Blowing snow has been discussed as a possible additional source for atmospheric Na<sup>+</sup>, raising the  
520 question, if it could be a source for atmospheric carbohydrates, too. During this study, the  
521 measurements of dFCHO and CCHO in five Arctic snow samples collected resulted in low values mostly  
522 below the limits of detection. This finding supports the conclusion that blowing snow does not serve  
523 as a competitive source for the emission of atmospheric marine carbohydrates.

### 524 3.3 Marine combined carbohydrates in fog

525 The concentrations of  $\text{Na}^+_{\text{fog, liquid}}$  (1.7–903  $\text{mg L}^{-1}$ ; mean =  $130 \pm 220 \text{ mg L}^{-1}$ ;  $n=22$ ) and  $\text{CCHO}_{\text{fog, liquid}}$   
526 (18–22000  $\mu\text{g L}^{-1}$ ; mean =  $1380 \pm 4600 \mu\text{g L}^{-1}$ ;  $n=22$ ) were very variable in fog water (**Table SI 2**).  
527 Atmospheric concentrations of these chemical constituents in fog droplets (indicated by the index  
528 ‘fog,atmos’) can be calculated under consideration of the liquid water content (LWC) during the fog  
529 events. Since LWC was not measured during PS106 directly, the LWC was approximated from the  
530 measured CCN concentrations at the lowest quality assured supersaturation of 0.15% and an assumed  
531 average droplet diameter of 17  $\mu\text{m}$ . This approach resulted in LWCs of  $0.62 \pm 0.39 \text{ g m}^{-3}$  for the fog  
532 collected over the North Sea and Norwegian Sea, and  $0.10 \pm 0.09 \text{ g m}^{-3}$  for the fog over the Arctic Ocean  
533 (Hartmann et al., 2021). Following this approach, atmospheric concentrations in fog ranged between  
534 0.12 and 150  $\mu\text{g m}^{-3}$  (mean =  $25 \pm 43 \mu\text{g m}^{-3}$ ;  $n=16$ ) for  $\text{Na}^+_{\text{fog, atmos}}$ , and between 3 and 4300  $\text{ng m}^{-3}$   
535 (mean =  $390 \pm 1100 \text{ ng m}^{-3}$ ;  $n=16$ ) for  $\text{CCHO}_{\text{fog, atmos}}$ , respectively. These atmospheric concentrations in  
536 fog are for both  $\text{Na}^+_{\text{fog, atmos}}$  and  $\text{CCHO}_{\text{fog, atmos}}$  by one to three orders of magnitude higher than the  
537 atmospheric concentrations in aerosols discussed in section 3.2. This divergence may be explained by  
538 the following:

- 539 - Fog scavenging is a transfer process of aerosol particles into the liquid phase of fog droplets  
540 (Gilardoni et al., 2014). As fog forms and grows, it can capture aerosol particles in the air and  
541 increase their concentration within the fog droplets. This could lead to higher atmospheric  
542 concentrations of aerosol particle compounds, especially for the water-soluble and  
543 hygroscopic ones, inside the fog compared to the surrounding air.
- 544 - The activation of aerosol particles to fog droplets is a process dominated by particle size with  
545 larger particles tending to activate first. It is conceivable that SSA particles larger than 10  $\mu\text{m}$ ,  
546 usually few in number, but with a large mass contribution, were available near the sea surface,  
547 where sampling occurred. These SSA particles were activated into fog droplets and contributed  
548 significantly to the  $\text{Na}^+$  and CCHO in the fog. In contrast, aerosol sampling was restricted by  
549 the Berner impactor’s 10  $\mu\text{m}$  diameter cut-off neglecting the larger particles in the  
550 consideration.
- 551 - The LWC values were not measured but estimated, which could be a source of errors. This  
552 approach resulted in values representing rather the upper limit of LWC values typically  
553 reported for Arctic summer fog (0.001-0.17  $\text{g m}^{-3}$  (Kumai, 1973)) or sea fog (0.02-0.1  $\text{g m}^{-3}$   
554 (Herrmann et al., 2015)), but appear within a realistic range. Consequently, they are likely not  
555 responsible for the large difference between aerosol and fog concentrations of several orders  
556 of magnitude.

557 Since both, organic and inorganic constituents, showed higher atmospheric concentrations in  
 558 fog/clouds compared to ambient aerosol particles, we conclude that a physical phenomenon, such as  
 559 fog scavenging, might explain this observation and not an in-situ formation within the cloud droplets.  
 560 Similar to the findings of this study discussing marine CCHO and Na<sup>+</sup> in Arctic fog, Triesch et al. (2021a)  
 561 found strikingly high concentrations of free amino acids (FAA) and Na<sup>+</sup> in marine clouds compared to  
 562 aerosol particles both collected on top of the Mt. Verde on Cape Verde as shown in **Table 1**.

563 While *d*FCHO<sub>fog</sub> and derivatives, such as anhydrosugars and sugar alcohols, have been readily reported  
 564 for fog water with terrestrial and marine background (Dominutti et al., 2022), we here present for the  
 565 first time ambient CCHO concentrations in marine fog.

566 **Table 1.** Atmospheric concentrations of selected SSA constituents in fog/clouds compared to ambient aerosol particles during  
 567 marine field studies.

Chemical constituent	Fog/cloud	PM <sub>10</sub>	Sampling location	Sampling height	Sampling period	Reference
	(ng m <sup>-3</sup> )	(ng m <sup>-3</sup> )		(m a.s.l.) <sup>h</sup>		
<i>d</i> FCHO	9.2–52 <sup>a,b</sup>	–	Reunion	1760 <sup>d</sup>	March–April 2019	Dominutti et al. (2022)
	1.5–1040 (mean:80±260)	<LOD–2.0	Arctic	25 <sup>e</sup>	May–July 2017	<b>this study</b>
CCHO	3–4300 (mean:390±1100)	0.5–4.7	Arctic	25 <sup>e</sup>	May–July 2017	<b>this study</b>
FAA	11–490	1.0–4.8	Cape Verde	744 <sup>f</sup>	Sept.–Oct. 2017	Triesch et al. (2021a)
	6–79 <sup>b</sup>	–	Reunion	1760 <sup>d</sup>	March–April 2019	Dominutti et al. (2022)
	(µg m <sup>-3</sup> )	(µg m <sup>-3</sup> )		(m a.s.l.) <sup>h</sup>		
Na <sup>+</sup>	1.6–7.2	0.17–0.40	Cape Verde	744 <sup>f</sup>	Sept.–Oct. 2017	Triesch et al. (2021a)
	0.1–2.2 <sup>b</sup>	–	Reunion	1760 <sup>d</sup>	March–April 2019	Dominutti et al. (2022)
	0.014–0.063 <sup>c</sup>	–	Arctic	180–374 <sup>g</sup>	Aug.–Sept. 2018	Zinke et al. (2021)
	0.12–150 (mean:25±43)	0.012–0.77	Arctic	25 m <sup>e</sup>	May–July 2017	<b>this study</b>

568 <sup>a</sup>only includes free glucose and rhamnose; sugar alcohols and anhydrosugars were not included for this table. <sup>b</sup>values were  
 569 calculated from LWCs, molecular weights and concentrations in fog water given within the reference; terrestrial contributions  
 570 are likely. <sup>c</sup>calculated from concentration in fog water and an assumed LWC of 0.1 g m<sup>-3</sup>. <sup>d</sup>Piste Omega. <sup>e</sup>RV *Polarstern*. <sup>f</sup>Mt.  
 571 Verde. <sup>g</sup>tethered balloon, <sup>h</sup>'m a.s.l.' abbreviates 'meters above sea level'.

### 572 3.4 Chemo-selective sea-air transfer of marine carbohydrates

573 The chemo-selective sea-air transfer of organics towards inorganic sea salt constituents has been  
 574 described both in tank and ambient field studies for organic carbon in general (Gantt et al., 2011;  
 575 Hoffman and Duce, 1976; van Pinxteren et al., 2017) or several chemical constituents, such as  
 576 carbohydrates (Hasenecz et al., 2020; Schill et al., 2018; Zeppenfeld et al., 2021a), lipids (Triesch et al.,  
 577 2021b) and free and combined amino acids (Triesch et al., 2021a, c). The calculation of dimensionless  
 578 ratios between the concentrations of the examined organic parameter and  $\text{Na}^+$  allows a comparison  
 579 of aquatic and atmospheric samples within the marine environment. **Figure 6** shows the  $\text{CCHO}/\text{Na}^+$   
 580 ratios for the bulk and SML in the four sea-ice-related sea surface compartments, size resolved aerosol  
 581 particles and fog water collected during the PS106 cruise.

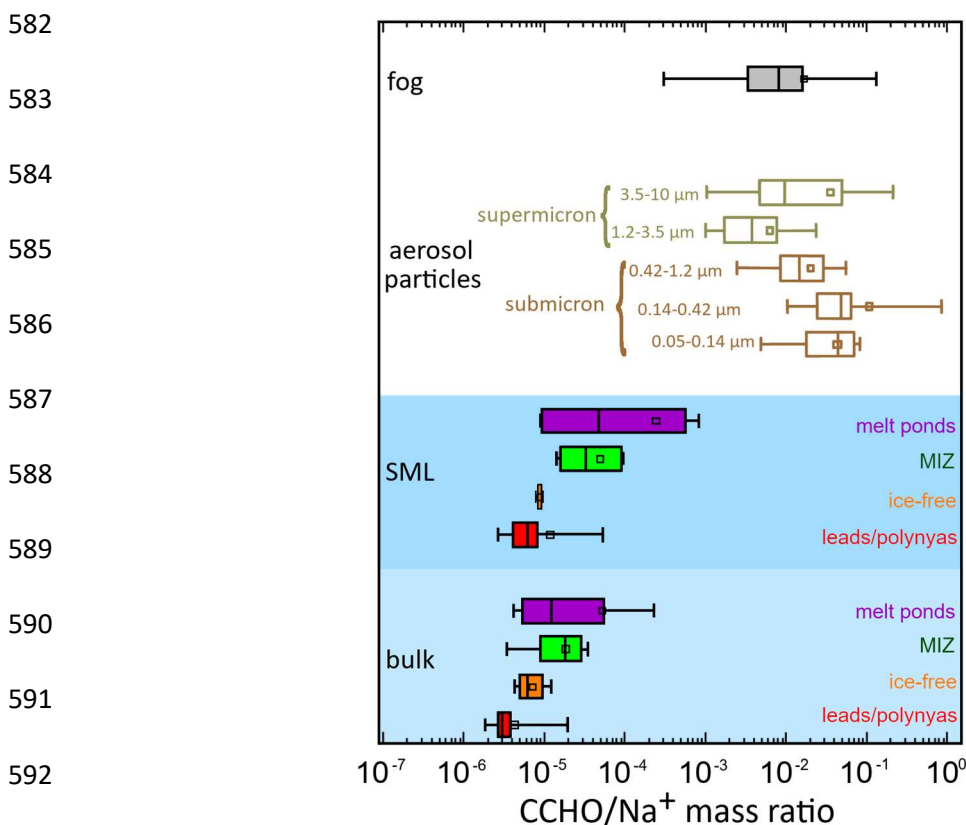


**Figure 6.** CCHO/Na<sup>+</sup> ratios for CCHO in Arctic fog, size-resolved aerosol particles and the surface seawater (SML and bulk) from melt ponds, the marginal ice zone (MIZ), the ice-free ocean and leads/polynyas from the pack ice.

593 **Wide range of CCHO/Na<sup>+</sup> ratios in Arctic surface seawater.** In the surface seawater samples of this  
 594 study, the CCHO/Na<sup>+</sup> ratios spanned from  $2 \times 10^{-6}$  to  $8 \times 10^{-4}$ , representing a wider range than those  
 595 found in the Southern Ocean ( $9 \times 10^{-7}$  and  $3 \times 10^{-5}$ ; Zeppenfeld et al., 2021). While the ratios in the SML  
 596 and bulk water in general ranged in the same orders of magnitude, large differences were observed in  
 597 the individual Arctic sea-ice-related sea surface compartments. In the SML, lowest median values were  
 598 found in the leads/polynyas and ice-free ocean samples with  $6 \times 10^{-6}$  and  $9 \times 10^{-6}$ , respectively, while  
 599 higher median values appeared in the SML of the MIZ ( $3 \times 10^{-5}$ ) and melt ponds ( $4 \times 10^{-5}$ ), or even

600  $6 \times 10^{-4}$ , when only aged melt ponds were considered. This large variability of CCHO/Na<sup>+</sup> ratios can be  
601 explained by the variable content of CCHO (high CCHO content in aged melt ponds & MIZ versus lower  
602 CCHO content in ice-free ocean & leads/polynyas) and Na<sup>+</sup> (low salinity in the SML of melt ponds versus  
603 higher salinities in ice-free ocean & leads/polynyas & MIZ) in the different sea-ice-related sea surface  
604 compartments. It can be expected, that the different CCHO/Na<sup>+</sup> ratios in the individual seawater  
605 compartments impacted the corresponding CCHO/Na<sup>+</sup> ratios in fog and aerosol particles during the  
606 sea-air transfer, and consequently the enrichment factors for the sea-air transfer ( $EF_{aer}$ ,  $EF_{fog}$ ), which  
607 are calculated from those ratios.

608 ***Air mass history influences CCHO<sub>aer</sub>/Na<sup>+</sup><sub>aer</sub> ratios in Arctic aerosol particles.*** In contrast to the  
609 seawater samples, CCHO<sub>aer</sub>/Na<sup>+</sup><sub>aer</sub> ratios were much higher for aerosol particles considering the size  
610 resolution ( $1 \times 10^{-3}$ – $9 \times 10^{-1}$ ) supporting the concept of the chemo-selective enrichment of  
611 carbohydrates towards Na<sup>+</sup> during the transfer from the ocean into the atmosphere. In this context,  
612 submicron particles showed much higher median ratios of  $4 \times 10^{-2}$  (0.05–0.14 μm) and  $4 \times 10^{-2}$   
613 (0.14–0.42 μm) than supermicron particles with  $4 \times 10^{-3}$  (1.2–3.5 μm) and  $1 \times 10^{-2}$  (3.5–10 μm).  
614 Regarding PM<sub>10</sub> (sum of all five Berner stages), the CCHO<sub>aer,PM10</sub>/Na<sup>+</sup><sub>aer,PM10</sub> ratios varied much more in  
615 the Arctic study presented here ( $2 \times 10^{-3}$ – $2 \times 10^{-1}$ , see **Table SI 1**) than in the ice-free part of the Southern  
616 Ocean ( $8 \times 10^{-4}$ – $7 \times 10^{-3}$ ; Zeppenfeld et al. (2021b)).

617 During four aerosol sampling periods (24/05/17–26/05/17; 26/05/17–29/05/17; 29/05/17–01/06/17;  
618 19/06/17–25/06/17), air masses had predominantly passed over the ice-free ocean (45–100% of the  
619 12 hours prior to sampling, as shown in **Table SI 1 & Figure SI 2**). Interestingly, these periods exhibited  
620 the lowest CCHO<sub>aer,PM10</sub>/Na<sup>+</sup><sub>aer,PM10</sub> ratios ( $2 \times 10^{-3}$ – $9 \times 10^{-3}$ , detailed in **Table SI 1**), values that are  
621 strikingly similar to those observed in the ice-free Southern Ocean. In contrast, higher ratios were  
622 found, when the air masses had rested a significant time over the pack ice or the MIZ. This could be an  
623 indication that the chemical composition of the sea-ice-related sea surface compartments, here the  
624 ice-free ocean with low CCHO/Na<sup>+</sup> ratios, strongly influences the relative composition of aerosol  
625 particles. In contrast, the influence of the MIZ, pack ice and melt ponds exhibiting quite different  
626 chemical, physical and biological properties on CCHO<sub>aer,PM10</sub>/Na<sup>+</sup><sub>aer,PM10</sub> could not be resolved in further  
627 details following this approach using back-trajectory calculations and satellite data. This is certainly  
628 due to the proximity of these sea-ice-related sea surface compartments on a small spatial scale  
629 (especially melt ponds in direct vicinity to open leads), the long sampling periods of aerosol particles,  
630 the lacking knowledge of deposition rates, the effect of wind on wave propagation and bubble bursting  
631 processes within the individual sea-ice-related sea surface compartments and missing data on the  
632 biological activities in individual melt ponds.



633 **Similar CCHO/Na<sup>+</sup> ratios in aerosol particles and fog.** For fog, CCHO<sub>fog</sub>/Na<sup>+</sup><sub>fog</sub> ratios ranged from  
634  $3 \times 10^{-4}$  to  $1 \times 10^{-1}$ , which covers the same orders of magnitude of aerosol particles. Even though absolute  
635 atmospheric concentrations of CCHO are much higher in fog than in aerosol particles possibly due to  
636 fog scavenging (as discussed in 3.3), the CCHO/Na<sup>+</sup> ratios were similar. This strongly implies that  
637 CCHO<sub>fog</sub> actually originated from the ambient marine aerosol particles. The attempt to find matches or  
638 common trends between aerosol particles and the fog in individual samples was not successful,  
639 certainly due to the very different resolutions of sampling times and in addition due to the probability  
640 of fog droplets containing aerosol particles bigger than 10 μm.

641 **Calculated EF<sub>aer</sub> and EF<sub>fog</sub> depend on the sea-ice-related marine source under consideration.** EF<sub>aer</sub> and  
642 EF<sub>fog</sub> are calculated as a quotient between the CCHO/Na<sup>+</sup> ratios in the size-resolved aerosol  
643 particles/fog and the corresponding bulk water. The CCHO/Na<sup>+</sup> ratios in the Arctic seawater of this  
644 study were very variable depending on the regarded sea-ice-related sea surface compartment  
645 environment, as well in the aerosol particles and in fog water. This fact strongly impacted the resulting  
646 hypothetical EF<sub>aer</sub> and EF<sub>fog</sub>, enabling calculated values ranging between 10<sup>1</sup> and 10<sup>4</sup> for supermicron  
647 aerosol particles, between 10<sup>2</sup> and 10<sup>5</sup> for submicron particles and between 10<sup>0</sup> and 10<sup>4</sup> for fog  
648 depending on which sea-ice-related sea surface compartment was assumed as the marine source of  
649 SSA as shown in **Figure 7**. Due to missing information, including SSA emission fluxes from the four sea-  
650 ice-related compartments, aerosol deposition rates, biological activities in melt ponds, wind effects on  
651 wave propagation and bubble bursting, and the comparative importance of melt ponds versus open  
652 leads (which are in close proximity, making it difficult to resolve them in back-trajectory analyses) as  
653 SSA sources – we didn't perform calculations based on the back-trajectory history of each atmospheric  
654 sample. Instead, subsequent calculations for EF<sub>aer</sub> and EF<sub>fog</sub> employed a hypothetical approach,  
655 assessing the range of enrichment factors by considering only one of the four sea-ice-related  
656 compartments—represented by the corresponding median CCHO<sub>bulk</sub>/Na<sup>+</sup><sub>bulk</sub> ratios—as the only source,  
657 while excluding the others.

658 Lower atmospheric EFs were calculated when aged melt ponds (EF<sub>aer,super</sub>=19–750; EF<sub>aer,sub</sub>=127–5100;  
659 EF<sub>fog</sub>=5–2400) or the MIZ (EF<sub>aer,super</sub>=60–2310; EF<sub>aer,sub</sub>=390–16000; EF<sub>fog</sub>=17–7400) were assumed as  
660 the only (theoretical) source of CCHO and Na<sup>+</sup>, while higher values were found with the ice-free ocean  
661 (EF<sub>aer,super</sub>=175–6800; EF<sub>aer,sub</sub>=1100–46000; EF<sub>fog</sub>=50–22000) or open leads/polynyas  
662 (EF<sub>aer,super</sub>=360–14000; EF<sub>aer,sub</sub>=2360–95000; EF<sub>fog</sub>=103–44600). It is important to note that EFs were  
663 most consistent with results from other CCHO sea-air transfer studies in the tank (Hasenecz et al.,  
664 2020) and the field (Zeppenfeld et al., 2021a), when aged melt ponds or the MIZ were considered as  
665 the only emission source. If leads/polynyas and the ice-free ocean were regarded as the only emission  
666 source, higher EF<sub>aer</sub> and EF<sub>fog</sub> values were obtained, and hence a possible overestimation of the

667 mechanistic process of enrichment. As the results on back-trajectory calculations and sea ice maps  
 668 demonstrated (Table SI 1 & Figure SI 2), most air masses were exposed to several of the sea-ice-related  
 669 sea surface compartments before sampling. Consequently, none of the Arctic sea-ice-related sea  
 670 surface compartments discussed above should be overlooked when discussing of sea-air transfer of  
 671 organic substances.

672 During the same Arctic field campaign, Hartmann et al. (2021) investigated INP in ambient aerosol  
 673 particles and compared it to bulk and SML in seawater from all the different sea-ice-related sea surface  
 674 compartments using similar  $EF_{aer}$  calculations as reported here. They concluded that an enrichment of  
 675 3 to 5 orders of magnitude was necessary during the sea-air transfer to fully attribute atmospheric INP  
 676 to oceanic sources. Here, we show that such high  $EF_{aer}$  and  $EF_{fog}$  for organics, and hence marine  
 677 biogenic INP, can be calculated, e.g. when open leads/polynyas were referred to as the only oceanic  
 678 source. In summary, Arctic air masses have been impacted by different types of sea-ice-related sea  
 679 surface compartments before sampling, whereas it is still unclear which one has the biggest effect on  
 680 the chemical composition of the marine aerosol particles. This aspect should be considered when the  
 681 marine SSA constituents are modelled for the Arctic from remote sensing data.

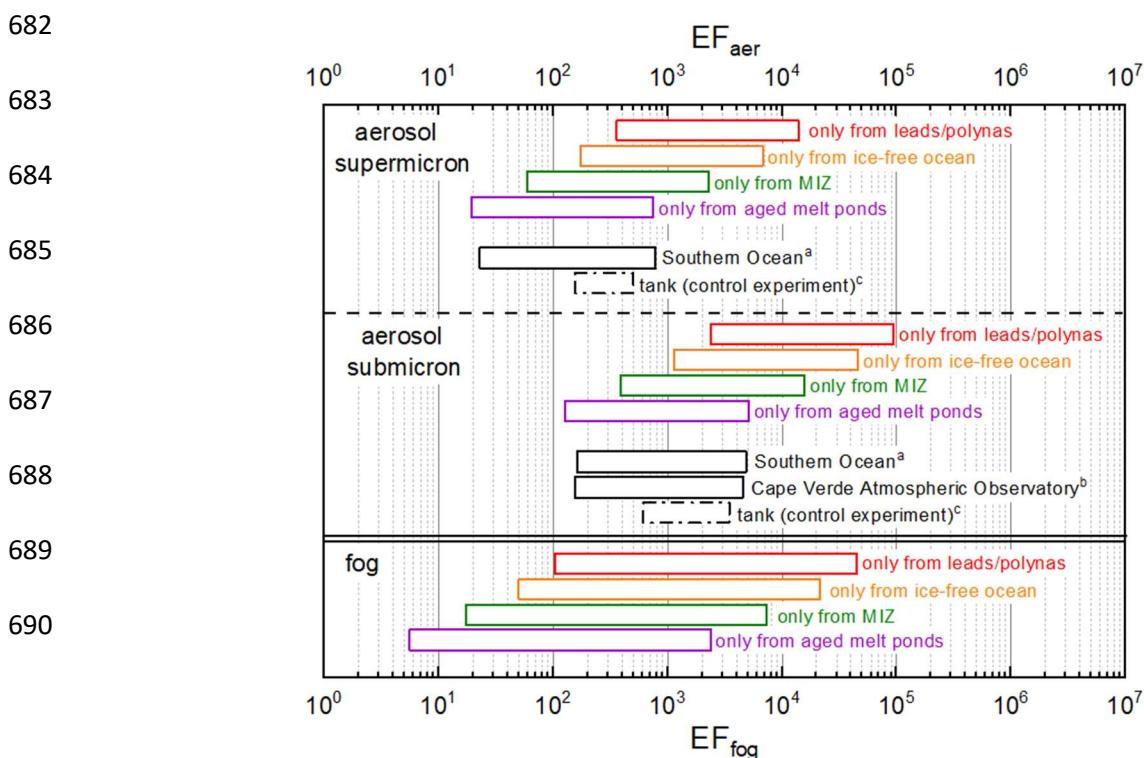


**Figure 7.** Range of calculated hypothetical enrichment factors  $EF_{aer}$  and  $EF_{fog}$  assuming either leads/polynyas, the ice-free ocean, the MIZ or aged melt ponds as the only marine source for the sea-air transfer of CCHO in the Arctic. For the calculation of  $EF_{aer}$  and  $EF_{fog}$ , the minimum and maximum values of the  $CCHO_{aer/fog}/Na^+_{aer/fog}$  ratios and the median values of  $CCHO_{bulk}/Na^+_{bulk}$  were used. The  $EF_{aer}$  values of this study were compared with the results of a) the field study conducted in the Southern Ocean by Zeppenfeld et al. (2021), b) the field study conducted at Cape Verde Atmospheric Observatory (CVAO) by van Pinxteren et al. (2023) and c) the results of the CCHO tank study by Hasenecz et al. (2020) without any addition of heterotrophic bacteria (control experiment). Here,  $EF_{aer}$  values were calculated from the experimental data published by Hasenecz et al. (2020b).

### 691 **3.5 Atmospheric aging of marine carbohydrates**

692 To resolve the fate of marine carbohydrates in the atmosphere after their ejection from the ocean, the  
693 relative molar contributions of monosaccharides to CCHO were compared between the bulk and SML  
694 from the leads/polynyas, MIZ, ice-free ocean and melt pond samples, as well as the sub-and  
695 supermicron aerosol particles and fog water (**Figure 8**). The composition of marine carbohydrates in  
696 seawater strongly depends on the dominating microbial species, season, diagenetic state, availability  
697 of nutrients and environmental stress factors (Engbrodt, 2001; Goldberg et al., 2011) leading to a  
698 natural variability among individual samples even within small spatial scales. Consequently, to enable  
699 the direct comparison of seawater with atmospheric samples of this field study with an elevated level  
700 of statistical certainty, here we compare the mean values of the entire data set, instead of individual  
701 samples. Finally, in addition to the changes of the monosaccharide patterns of CCHO, the systematic  
702 degradation of CCHO to *d*FCHO was observed in the atmosphere and will be discussed within this  
703 section.

704 ***CCHO composition in different sea-ice-related sea surface compartments and depths is similar.*** In  
705 seawater (bulk and SML), glucose (means= 35–48 mol%), galactose (means= 13–18 mol%) and xylose  
706 (means= 7–16 mol%) dominated the CCHO composition followed by smaller contributions of other  
707 neutral sugars, amino sugars, uronic acids and muramic acid (**Figure 8**). Considering the natural  
708 variability among individual samples, there were no significant differences in means between the bulk  
709 and SML, nor between the lead/polynya, MIZ, ice-free ocean and melt pond samples. Variations were  
710 observed between the dissolved and particulate fractions (**Figure SI 3**), nevertheless the combined  
711 carbohydrates within all sea-ice-related sea surface compartments followed the same pattern of the  
712 predominance of glucose, galactose and xylose. Overall, the relative monosaccharide compositions of  
713 glucose > (galactose ≈ xylose) > other (neutral or charged) monosaccharides of the seawater samples  
714 from this Arctic study appear similar to the monosaccharide compositions investigated in the SML and  
715 bulk water from the Central Arctic Ocean (Gao et al., 2012) and at the western Antarctic peninsula  
716 (Zeppenfeld et al., 2021a), the meltwater of Arctic multiyear sea ice (Amon et al., 2001) and the  
717 epipelagic water from the Ross Sea (Kirchman et al., 2001).

718 ***Less galactose, but more muramic acid in atmospheric CCHO<sub>aer</sub> and CCHO<sub>fog</sub>.*** Atmospheric samples  
719 showed a different monosaccharide pattern within the hydrolyzed CCHO in comparison to the  
720 seawater and melt pond samples. While glucose (means= 41 mol% for fog; 50 mol% for submicron and  
721 60 mol% for supermicron aerosol particles) and xylose (means= 16; 15 and 15 mol%) still prevailed  
722 over the relative monosaccharide pattern, the contribution of galactose (means= 6; 3 and 3 mol%) was  
723 strongly reduced, both in fog and aerosol particles. On the other hand, the ratio of muramic acid was

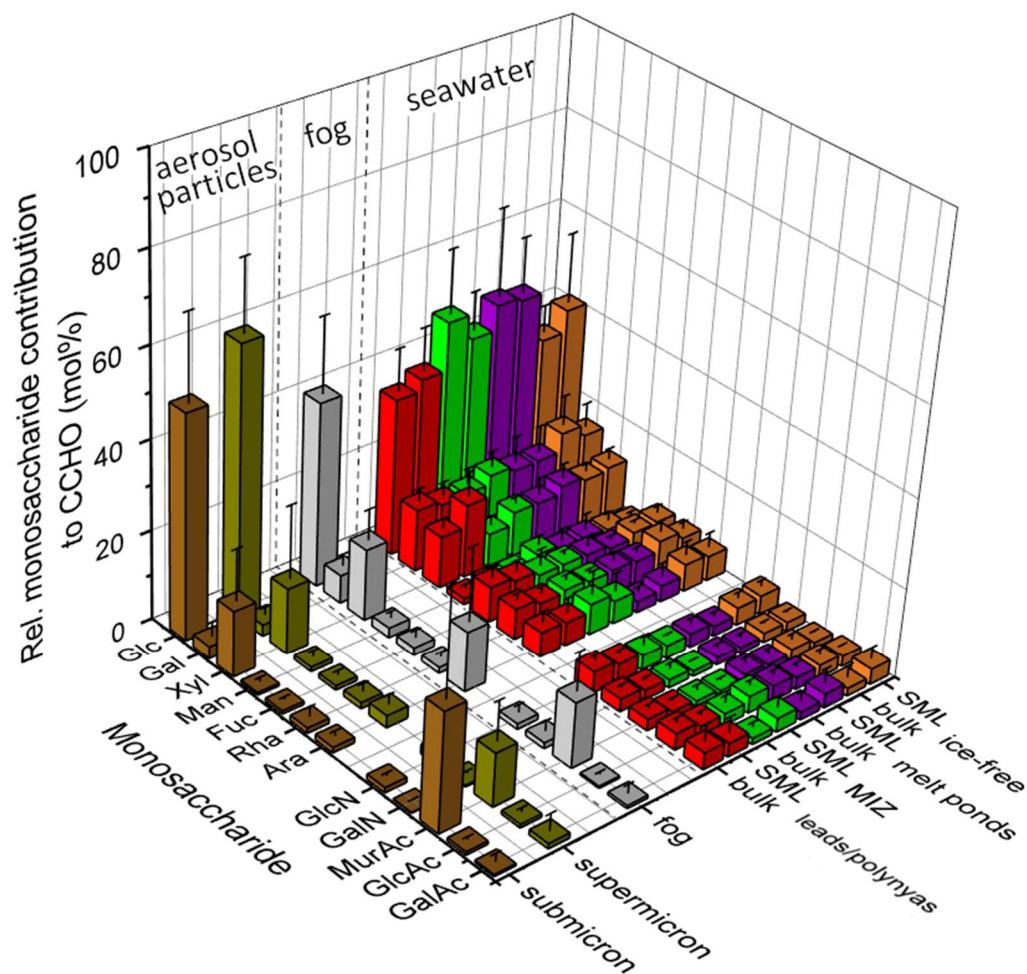


**Figure 8.** Relative monosaccharide composition of combined carbohydrates (CCHO) after acid hydrolysis in sub-/ supermicron aerosol particles, fog water, bulk and SML samples from the leads and polynyas within the pack ice, the MIZ, the ice-free ocean and young and aged melt ponds. The 3D bar chart shows the averages and standard deviations of the relative contributions. Glc: glucose, Gal: galactose, Xyl: xylose, Man: mannose, Fuc: fucose, Ara: arabinose, GlcN: glucosamine, GalN: galactosamine, MurAc: muramic acid, GlcAc: glucuronic acid, GalAc: galacturonic acid.

724 strongly elevated in aerosol particles (means= 12 and 26 mol%) and fog water (mean= 14 mol%) in  
 725 comparison to the oceanic samples (means= 0.9–2.6 mol%). These differences of the relative  
 726 monosaccharide contributions to CCHO among the seawater and the atmospheric samples described  
 727 within this study are in good agreement with the sea-air transfer investigations conducted in the  
 728 Southern Ocean at the western Antarctic peninsula (Zeppenfeld et al., 2021a). Consequently, the  
 729 occurring phenomenon might be independent from the sampling location and could be explained by  
 730 three possible atmospheric processes, such as (1) a chemo-selective sea-air transfer of certain oligo-  
 731 or polysaccharides over others, (2) an atmospheric transformation due to abiotic chemical reactions  
 732 or (3) an atmospheric transformation due to microbiological activities. Among these possible  
 733 pathways, Zeppenfeld et al. (2021) presumed the secondary atmospheric transformation caused by  
 734 microbiological metabolism as the most probable or at least most dominant one supported by the  
 735 prevalence of muramic acid, an amino sugar acid naturally occurring in bacterial cell walls (Mimura

736 and Romano, 1985; Sud and Tyler, 1964), and the very selective absence of certain monosaccharides  
737 in the CCHO<sub>aer</sub> in aerosol particles as it was observed in this Arctic study as well.

738 **Formation of combined arabinose in fog.** A comparison of the monosaccharide composition of aerosol  
739 particles and fog water showed great similarity regarding dominant contributions from glucose, xylose  
740 and muramic acid. It seems plausible that the fog water droplets contained the same inorganic and  
741 organic compounds found in the SSA particles assuming that SSA particles activated the formation of  
742 fog droplets as CCN due to their rather large diameters and high hygroscopicity. Apart from that,  
743 however, a significant difference was observed in the increased relative contribution of arabinose in  
744 fog (mean= 13 mol%) compared to aerosol particles (means= 1.2 and 2.7 mol%) indicating a formation  
745 of arabinose in the liquid phase. During a marine microcosm experiment performed by Hasenecz et al.  
746 (2020), a strong link was observed between the release of arabinose-containing polysaccharides in  
747 form of EPS and the presence of heterotrophic bacteria and stressed phytoplankton. Furthermore, a  
748 strain of the psychrotolerant marine bacterium *Pseudoalteromonas* sp. has been shown to produce  
749 EPS mainly composed from glucose, arabinose and xylose (Casillo et al., 2018; Qin et al., 2007).  
750 Consequently, the release of arabinose-containing EPS in fog could be a plausible protection  
751 mechanism of microorganisms contained within a droplet against freezing damage under low Arctic  
752 temperatures.

753 **Indication for microbial activities in the atmosphere.** Intact bacterial cells at atmospheric  
754 concentrations between  $5 \times 10^2$  and  $8 \times 10^4$  cells  $m^{-3}$  for remote marine and ice-covered regions (Šantl-  
755 Temkiv et al., 2018; Mayol et al., 2017), cell-bound and free enzymes have been detected in ambient  
756 and nascent marine super- and submicron aerosol particles during several field and tank studies (Aller  
757 et al., 2005; Hasenecz et al., 2020; Malfatti et al., 2019; Marks et al., 2001; Rastelli et al., 2017; Šantl-  
758 Temkiv et al., 2020; Uetake et al., 2020). For surviving in this hostile environment, some of these  
759 microbes have developed a remarkable resilience towards extreme environmental stressors, such as  
760 high UV radiation, radical exposure, changing osmolarity, freezing temperatures and desiccation. As  
761 survival strategies could serve the selective enzymatic consumption of airborne labile carbohydrates  
762 explaining the here observed loss of galactose and the persistence of xylose, the release of protecting  
763 biofilms from EPS, carotenoid pigmentation or the formation of own precipitating hydrometeors by  
764 enabling condensation on a surface as a CCN or freezing by IN active surfaces to reduce their  
765 atmospheric residence time (Delort et al., 2010; Matulová et al., 2014; Šantl-Temkiv et al., 2020).  
766 Consequently, an enzymatic transformation might serve as a plausible explanation for the selective  
767 removal of certain monosaccharides within CCHO<sub>aer</sub> and CCHO<sub>fog</sub> observed here. However, the survival  
768 and the metabolic activity of microorganisms is restricted by the presence of water (Ervens and Amato,  
769 2020; Haddrell and Thomas, 2017) identifying liquid hydrometeors or fresh SSA as the most biologically

770 active atmospheric hotspots. In contrast to most of the ambient aerosol particles, fog droplets provide  
771 enough water essential for bacterial activities. However, they might freeze under Arctic sub-zero  
772 temperatures possibly causing damage to the microbial cells, which might explain an in-situ formation  
773 of a protecting biofilm from arabinose-containing EPS. In a previous Arctic study, Orellana et al. (2011)  
774 readily detected microgels in aerosol particles, cloud and fog water most likely emitted from the  
775 surface water and the SML via bubble bursting. Indications for an in-situ generation of marine  
776 microgels in fog water as an additional source to the primary release from the ocean by bubble bursting  
777 have been observed by van Pinxteren et al. (2022) in the tropical Atlantic Ocean.

778 The selective sea-air transfer of certain carbohydrates over others and the abiotic degradation as  
779 further possible pathways to the biotic transformation of marine CCHO<sub>aer</sub> have been discussed in detail  
780 in Zeppenfeld et al. (2021), but do not appear, based on the current state of knowledge, as likely  
781 explanations of the very selective CCHO degradation and formation of other CCHO observed here.  
782 More future lab and mesocosm experiments are required to elucidate the contribution of each of these  
783 processes. Finally, the similarity between the carbohydrate compositions of fog water and aerosol  
784 particles, both two atmospheric compartments collected with different instrumentation, allows to rule  
785 out artefacts of the different sampling and extraction techniques as a reason for the observed  
786 differences to the seawater.

787 ***Depolymerization of CCHO to dFCHO, seawater versus atmosphere.*** Free glucose, by far the most  
788 prevailing monosaccharide among dFCHO in seawater, ranged between 0.6 and 51  $\mu\text{g L}^{-1}$  during the  
789 PS106 cruise in the bulk and the SML (Zeppenfeld et al., 2019a). Thus, dFCHO/CHO ratios, meaning the  
790 contribution of sugar monomers to all marine carbohydrates measured in this study, varied between  
791 1–14% with an average of  $5\pm 3\%$ . Conversely, 86–99% (mean:  $95\pm 3$ ) of carbohydrates in the bulk and  
792 SML of ocean seawater and melt ponds were incorporated into an oligo- or polysaccharidic structure.  
793 CCHO can be hydrolyzed to dFCHO either in an acidic environment or enzymatically by heterotrophic  
794 bacteria (Arnosti, 2000; Panagiotopoulos and Sempéré, 2005). Seawater from the Arctic Ocean is  
795 slightly alkaline with reported pH values between 7.98 and 8.49 (Rérolle et al., 2016; Tynan et al.,  
796 2016), while the pH of melt pond water has been observed to be more variable from mildly acidic (6.1)  
797 to more alkaline (10.8) (Bates et al., 2014). In agreement with previous findings, the oceanic surface  
798 seawater (pH: 7.98–8.66), including the samples from the MIZ, ice-free ocean and open  
799 leads/polynyas, and the melt pond samples (pH: 7.26–8.62) were slightly alkaline in this study.  
800 Consequently, it is more plausible that the depolymerization of CCHO in seawater can be ascribed to  
801 bacterial activities rather than acid hydrolysis. Since dFCHO are readily resorbed by heterotrophic  
802 bacteria with high turnover rates (Ittekkot et al., 1981; Kirchman et al., 2001), concentrations of these  
803 monosaccharides are rather low in seawater.

804 In contrast, in aerosol particles, higher  $d\text{FCHO}/\text{CHO}$  ratios up to 35% occurred in some selected  
805 samples, which is much higher than in seawater, suggesting that CCHO might be depolymerized in the  
806 atmosphere. SSA particles are known to significantly acidify within minutes after their release due to  
807 the uptake of acidic gases, atmospheric aging reactions with sulfuric dioxide and water loss (Angle et  
808 al., 2021). In this context, the surface-to-volume ratio determines the efficiency of the acidification  
809 effect, which means that it is most pronounced for submicron SSA particles with reported pH values  
810 of 1.5–2.6 within a few minutes in a tank study (Angle et al., 2021), and less pronounced for  
811 supermicron SSA particles or cloud droplets (Angle et al., 2022). Consequently, it is conceivable that  
812 an acid hydrolysis of  $\text{CCHO}_{\text{aer}}$  to monomeric  $d\text{FCHO}_{\text{aer}}$  occurs at the surface or within the bulk of SSA  
813 particles leading to quick atmospheric aging. However, due to analytical constraints, such as the limits  
814 of detections (LODs) of the methodology, the  $d\text{FCHO}$  in size-resolved aerosol particles could not be  
815 detected in all samples and the data availability is not strong enough to draw more conclusions for  
816 aerosol particles.

817 In fog, where LODs did not represent an issue due to the high concentrations,  $d\text{FCHO}/\text{CHO}$  ratios  
818 exceeding those in seawater were also observed, ranging from 1-60% (mean:  $27\pm 16\%$ ). The  
819 monosaccharide composition of  $d\text{FCHO}_{\text{fog}}$  was primarily made up of glucose, arabinose, fructose, and  
820 xylose, with minor contributions from glucosamine, galactose, mannose, rhamnose, and fucose. While  
821  $d\text{FCHO}_{\text{fog}}$  and  $\text{CCHO}_{\text{fog}}$  shared similar dominant monosaccharides, fructose was only present in  
822  $d\text{FCHO}_{\text{fog}}$ . This absence in  $\text{CCHO}_{\text{fog}}$  is attributed to fructose's low stability during the analytical  
823 preparation for CCHO analysis (Panagiotopoulos and Sempéré, 2005). As a result, fructose won't be  
824 further discussed. In this study, pH values of fog water ranged between 5.7 and 6.8, which is 1–2  
825 magnitudes more acidic than in seawater. Polysaccharides are known to depolymerize due to acid  
826 hydrolysis, especially at elevated temperatures. The pH-stability can be largely variable among the  
827 different polysaccharides; however, we are not aware of studies that have shown such fast  
828 depolymerizations, in the sense of time scales relevant for atmospheric lifetime of aerosol particles, at  
829 such mildly acid conditions and low temperatures as those of the Arctic atmosphere. Furthermore,  
830 there was no significant correlation between the pH and the  $d\text{FCHO}/\text{CHO}$  of these cloud samples.  
831 Consequently, there are no indications that the majority of CCHO was hydrolyzed inside the cloud  
832 droplets, however it might be conceivable that hydrolysis had readily occurred within the non-  
833 activated SSA particle where pH values were much lower.

834 Besides an acid hydrolysis induced by quick atmospheric acidification of SSA particles, atmospheric  
835 radicals, such as OH (Trueblood et al., 2019), or photolytic cleavages of glycosidic bonds (Kubota et al.,  
836 1976) could have contributed to the degradation of atmospheric CCHO to monomeric  $d\text{FCHO}$  in SSA  
837 and marine fog. For these processes, however, still hardly any systematic lab studies have been

838 conducted for the plurality of marine polysaccharides, which makes a classification of the meaning of  
839 these processes difficult. A preferred sea-air transfer of *d*FCHO over CCHO to explain this observation  
840 seems unlikely based on the missing enrichment of neutral *d*FCHO in contrast to the high  $EF_{aer}$  of CCHO  
841 shown in tank studies (Hasenecz et al., 2019, 2020). Finally, a microbial depolymerization of CCHO by  
842 extracellular enzymes in fog cannot be entirely ruled out considering that the activity of some  
843 polysaccharide-degrading enzymes, such as  $\alpha$ - and  $\beta$ -glucosidase, have been found to accelerate in  
844 seawater with increasing acidity (Piontek et al., 2010). However, this finding was conducted for a pH  
845 range only 0.3 pH units lower than the typical pH of seawater and it is not sure, if this finding can be  
846 transferred to the more acid conditions in aerosol particles and fog water.

847 ***Several aging processes in the atmosphere.*** We observed significant changes between the chemical  
848 composition of marine carbohydrates in the surface seawater, including the bulk and SML, and  
849 atmospheric carbohydrates, including aerosol particles and fog. Based on the changing  
850 monosaccharide composition pattern of CCHO with selective degradation and formation of specific  
851 monosaccharides within CCHO, we conclude microbial or enzymatic activities within the aerosol  
852 particles of fog droplets. Furthermore, the increasing contribution of *d*FCHO to the total carbohydrate  
853 pool in fog and aerosol particles might be attributed to a hydrolytic cleavage of the glycosidic linkages  
854 between monosaccharide units within the oligo- and polysaccharides after a quick atmospheric  
855 acidification of SSA particles. Consequently, atmospheric carbohydrates experience quick atmospheric  
856 aging, potentially due to both biological and abiotic processes, after their release from the ocean.  
857 Possibly, this could affect the CCN and INP properties of marine carbohydrates and hence the  
858 formation and properties of clouds.



### 859 3.6 Perspective assessment of CCHO via bio-optical parameters

860 The absorption of phytoplankton ( $a_{ph}$ ) and CDOM ( $a_{CDOM}$ ) are bio-optical parameters providing  
861 additional information about the chemical and microbiological history of the water masses within the  
862 particulate and dissolved phase, respectively. They can be measured on discrete water samples and  
863 can also be assessed as products from satellites (Lefering et al., 2017; Matsuoka et al., 2012, 2013;  
864 Röttgers et al., 2016). Here we tested, if  $a_{ph}$  or CDOM parameters correlate with CCHO in seawater to  
865 potentially enable the remote-sensing approximation of marine CCHO in seawater and potentially in  
866 the atmosphere.

867 **Good assessment of CCHO in seawater via  $a_{ph440}$ .**  $a_{ph440}$  derived from the phytoplankton absorption  
868 spectrum is directly related to the biomarker TChl-*a* indicating phytoplankton biomass (Bricaud et al.,  
869 2004; Phongphattarawat, 2016). The advantage of using  $a_{ph440}$  over pigment data, including TChl-*a*  
870 from full high-performance liquid chromatography (HPLC) analysis (e.g. Barlow et al., 1997; Taylor et  
871 al., 2011), is the lower need of sample volume for the analysis. This allows the determination of values  
872 in the SML samples as well (Zäncker et al., 2017), which are laborious to collect and therefore limited  
873 in availability. In this study,  $a_{ph440}$  strongly correlated with  $pCCHO$  ( $R=0.90$ ,  $p<0.001$ ) in bulk and SML  
874 samples (**Figure 9a**) showing a direct link with fresh phytoplankton biomass production. A similar link  
875 has been described before for TChl-*a* and  $pCCHO$  in the photic layer of the Ross Sea (Fabiano et al.,  
876 1993), in the ocean west of the Antarctic peninsula (Zeppenfeld et al., 2021a) and between TChl-*a* and  
877 the particulate form of laminarin, an algal polysaccharide, in Arctic and Atlantic water samples (Becker  
878 et al., 2020).  $dCCHO$  showed a good, but weaker correlation with  $a_{ph440}$  ( $R=0.66$ ,  $p<0.001$ ) than  
879  $pCCHO$ . This finding supports the assumption that  $pCCHO$  are rather freshly produced by local  
880 autotrophs, while the link between  $dCCHO$  with their primary production was already obscured by  
881 subsequent transformation processes resulting in a more recalcitrant, long-lived mix of  
882 macromolecules (Goldberg et al., 2011; Hansell, 2013; Keene et al., 2017). Nevertheless, CCHO, the  
883 sum from  $dCCHO$  and  $pCCHO$ , showed a high correlation with  $a_{ph440}$  ( $R=0.84$ ,  $p<0.001$ , **Figure 9b**)  
884 leading to the conclusion that this bio-optical parameter derived from the  $a_{ph}(\lambda)$  spectrum is suitable  
885 to assess the total amount of CCHO in the surface seawater of the different sea-ice-related sea surface  
886 compartments of the Arctic.

887 **Good assessment of CCHO in seawater via  $a_{CDOM350}$ .** In this study, high correlations were observed  
888 between  $dCCHO$  and  $a_{CDOM350}$  ( $R=0.66$ ,  $p<0.001$ , **Figure 10a**), and weaker correlations between  $dCCHO$   
889 and  $a_{CDOM443}$  ( $R=0.53$ ,  $p<0.001$ , **Figure 10b**). The better correlation at  $\lambda=350$  nm compared to 443 nm  
890 can be explained by the fact that  $a_{CDOM}$  exponentially decreases with wavelength. While absorption by  
891 CDOM is higher at  $\lambda=350$  nm, it is much closer to the method detection limit at  $\lambda=443$  nm and is

892 therefore more error-prone. However, with current satellite products only  $a_{CDOM}$  at 440 nm can be  
893 retrieved.

894 Previous studies reported strong correlations between  $a_{CDOM350}$  and dissolved organic carbon (DOC)  
895 in Arctic seawater (Gonçalves-Araujo et al., 2015; Spencer et al., 2009; Stedmon et al., 2011; Walker  
896 et al., 2013). Consequently, it is conceivable that  $dCCHO$ , an important constituent of DOC, shows good  
897 correlations as well. Surprisingly, the correlation between CCHO (sum of  $dCCHO$  and  $pCCHO$ ) and  
898  $a_{CDOM350}$  was strongest ( $R=0.85$ ,  $p<0.001$ , **Figure 10c**), indicating that CDOM retrieval from high-  
899 resolution satellite data could allow a good approximation of CCHO in Arctic seawater.

900

901

902

903

904

905

906

907

908

909

910

911

912

913

914

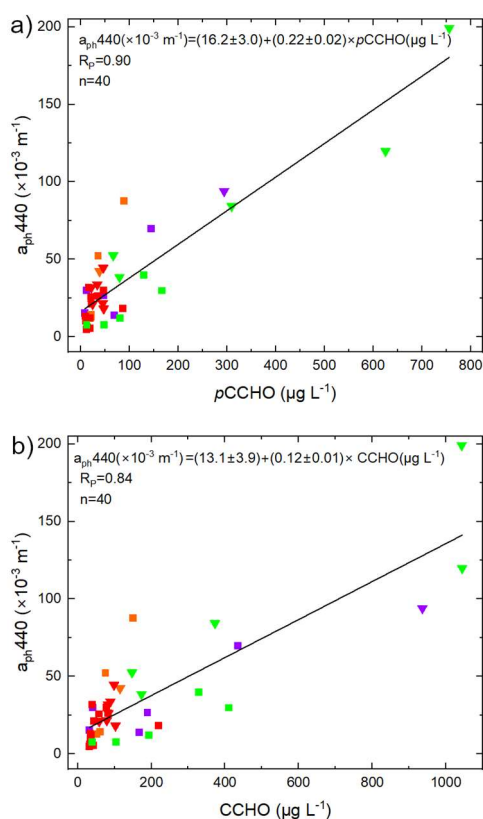


**Figure 9.** Correlation plots of  $a_{ph440}$  derived from PAB spectra against a)  $pCCHO$  and b) CCHO. Triangles: SML, squares: bulk. Green: marginal ice zone (MIZ), purple: melt ponds, orange: ice-free ocean, red: open leads/polynyas in the pack ice.

915

916

917

918

919

920

921  
 922  
 923  
 924  
 925  
 926  
 927  
 928  
 929  
 930  
 931  
 932  
 933  
 934  
 935  
 936  
 937  
 938

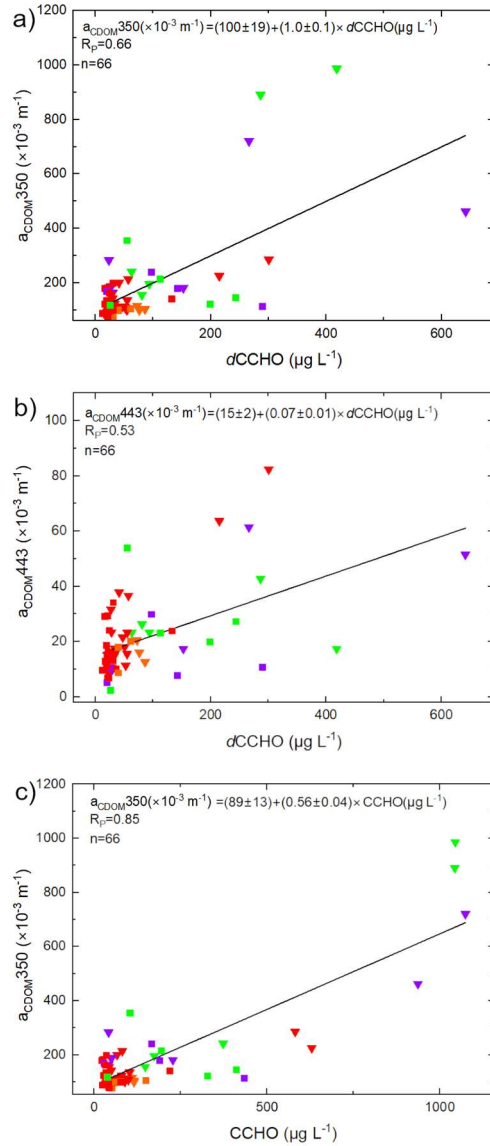


**Figure 10.** Correlation plots of a)  $a_{\text{CDOM}350}$  against  $d\text{CCHO}$ , b)  $a_{\text{CDOM}443}$  against  $d\text{CCHO}$  and c)  $a_{\text{CDOM}350}$  against  $\text{CCHO}$ . Triangles: SML, squares: bulk. Green: marginal ice zone (MIZ), purple: melt ponds, orange: ice-free ocean, red: open leads/polynyas in the pack ice.

## 939 **4. Summary and Atmospheric Implications**

940 We studied the sea-air transfer of marine carbohydrates from field samples collected in the Arctic  
941 during the PS106 campaign from May to July 2017. Large differences of absolute CCHO concentrations  
942 and SML enrichments were observed among the different sea-ice-related sea surface compartments  
943 (leads/polynyas within the pack ice, ice-free ocean, MIZ, melt ponds). CCHO<sub>aer</sub> were detected in the  
944 sub- and supermicron aerosol particles with indications for primary emissions from the sea through  
945 bubble bursting, though the correlations with the SSA tracer Na<sup>+</sup> and wind speed were possibly  
946 reduced due to the presence of sea ice influencing the wind-induced SSA emission mechanisms.  
947 Atmospheric CCHO and Na<sup>+</sup> concentrations in fog strongly exceeded those of the aerosol particles likely  
948 due to a physical phenomenon. Large enrichments of CCHO in aerosol and fog compared to bulk  
949 seawater were observed. The extent of these enrichments varied based on the type of sea-ice-related  
950 sea surface compartment assumed as the oceanic source for atmospheric CCHO. We observed a  
951 subsequent atmospheric aging of CCHO in the atmosphere, both in aerosol particles and fog, noticed  
952 by the selective loss and formation of certain monosaccharide units within CCHO suggesting selective  
953 enzymatic/microbial activities, and a depolymerization of CCHO to *d*FCHO, most measurable in fog  
954 water and likely due to abiotic degradation, e.g. acid hydrolysis. CCHO correlated well with bio-optical  
955 parameters, such as  $a_{ph440}$  from phytoplankton absorption and  $a_{CDOM350}$ . These parameters can be  
956 measured via remote sensing and may allow the retrieval of CCHO from satellite data, which  
957 potentially will enable an accurate modelling of atmospheric CCHO concentrations as soon as all  
958 emission and atmospheric aging processes are sufficiently understood. This study shows that the Arctic  
959 is a complex environment, where the diversity of sea-ice-related sea surface compartments needs to  
960 be considered as primary sources of marine CCHO or other organic compounds, and where these  
961 molecules can be transformed after their primary sea-air transfer by biological and abiotic processes  
962 in the atmosphere.

963 Marine carbohydrates are assumed to impact cloud properties by acting as CCN and INP (Alpert et al.  
964 2022; Leck et al., 2013; Orellana et al., 2011; van Pinxteren et al., 2022). Studying the chemical identity  
965 of those atmospheric nucleation particles, their emission mechanisms and their transformation due to  
966 atmospheric aging can strongly improve the understanding of the cloud formation in the Arctic, cloud  
967 microphysical properties, the radiation budget, cryosphere-ocean-atmosphere interactions and  
968 eventually feedback mechanisms in the frame of Arctic amplification. It can be assumed that within  
969 the warming Arctic, where sea ice extent is continuously shrinking, the MIZ area will expand (Strong  
970 and Rigor, 2013) and the number of biologically-active melt ponds will increase during the summer  
971 season in the next years. These new MIZ regions and melt ponds could potentially produce more  
972 marine carbohydrates than the ice-free ocean or open leads within the pack ice leading to enhanced

973 CCN and INP populations in the Arctic atmosphere serving as a still not well-explored feedback  
974 mechanism within Arctic amplification.

975 **Data availability.** All data are available on the public repository PANGAEA:  
976 <https://doi.org/10.1594/PANGAEA.962208> and <https://doi.org/10.1594/PANGAEA.932573> (for fog  
977 samples); <https://doi.org/10.1594/PANGAEA.962210> and <https://doi.org/10.1594/PANGAEA.932569>  
978 (for aerosol particles); <https://doi.org/10.1594/PANGAEA.961004> (for seawater samples).

979 **Author contribution.** SZ wrote the manuscript with contributions from MvP, MH, MZ, AB and HH. SZ,  
980 MvP and MH collected the field samples during the PS106 campaign. SZ performed the laboratory  
981 carbohydrate analysis and statistical evaluation. MZ and AB assessed the bio-optical parameters. All  
982 co-authors proofread and commented the manuscript.

983 **Competing interests.** The authors declare that they have no conflict of interest.

984 **Acknowledgements.** We gratefully acknowledge the funding by the Deutsche Forschungsgemeinschaft  
985 (DFG, German Research Foundation, Projektnummer 268020496–TRR 172) within the Transregional  
986 Collaborative Research Center “Arctic Amplification: Climate Relevant Atmospheric and Surface  
987 Processes, and Feedback Mechanisms (AC)<sup>3</sup>”. This research has been supported by the DFG SPP 1158,  
988 grant number 424326801 by enabling the access to melt pond data. We thank Andreas Macke and  
989 Hauke Flores, chief scientists for the RV *Polarstern* cruises PS106.1 and PS106.2 (expedition grant  
990 number AWI\_PS106\_00), and the captain and the crew of RV *Polarstern* for their support during the  
991 expedition from May to July 2017. We thank Andrea Haudek and Hartmut Haudek for the development  
992 and construction of the conditioning tube and the wind control system connected to the Berner  
993 impactor. We thank Anett Dietze, Susanne Fuchs and Anke Rödger for the mass, inorganic ion and  
994 OC/EC measurements. We acknowledge René Rabe and Sonja Wiegmann for supporting the  
995 preparation of PS106 chemical equipment and optical instrumentation, respectively, and Yangyang Liu  
996 for introducing the optical measurement procedure before PS106.

997 **Financial support.** This research has been supported by the Deutsche Forschungsgemeinschaft (DFG,  
998 German Research Foundation, Projektnummer 268020496–TRR 172) within the Transregional  
999 Collaborative Research Center “Arctic Amplification: Climate Relevant Atmospheric and Surface  
1000 Processes, and Feedback Mechanisms (AC)<sup>3</sup>” in subprojects B04 and C03.

## 1001 List of abbreviations

1002	$a_{\text{CDOM}}$	absorption coefficient by colored dissolved organic carbon
1003	aer	aerosol particles
1004	$a_{\text{NAP}}$	absorption coefficient by non-algal particles
1005	ANOVA	Analysis of Variance
1006	$a_{\text{p}}$	absorption coefficient by total particles
1007	$a_{\text{ph}}$	absorption coefficient by phytoplankton

1008	Ara	arabinose
1009	atmos	atmospheric concentrations
1010	C-CCHO	carbon contained within the combined carbohydrate
1011	CCHO	combined carbohydrates
1012	CCN	cloud condensation nuclei
1013	CDOM	colored dissolved organic matter
1014	CHO	carbohydrates
1015	<i>d</i> CCHO	dissolved combined carbohydrates
1016	<i>d</i> FCHO	dissolved free carbohydrates
1017	EF	enrichment factor
1018	EPS	exopolymeric substances
1019	ERDDAP	Environmental Research Division's Data Access Program
1020	FAA	free amino acids
1021	Fru	fructose
1022	Fuc	fucose
1023	Gal	galactose
1024	GalN	galactosamine
1025	GalAc	galacturonic acid
1026	Glc	glucose
1027	GlcAc	glucuronic acid
1028	GlcN	glucosamine
1029	HPAEC-PAD	high-performance anion-exchange chromatography with pulsed amperometric detection
1030	HPLC	high-performance liquid chromatography
1031	INP	ice nucleating particles
1032	LWCC	liquid waveguide capillary cell
1033	Man	mannose
1034	MIZ	marginal ice zone
1035	MurAc	muramic acid
1036	Na <sup>+</sup>	sodium ion
1037	NOAA	National Oceanic and Atmospheric Administration
1038	OC	organic carbon
1039	OM	organic matter
1040	PAB	particulate absorption
1041	<i>p</i> CCHO	particulate combined carbohydrates
1042	PM	particulate matter
1043	Rha	rhamnose
1044	SML	sea surface microlayer
1045	SSA	sea spray aerosol
1046	sub	submicron
1047	super	supermicron
1048	TChl- <i>α</i>	total chlorophyll <i>α</i>
1049	TEP	transparent exopolymer particles
1050	QFT-ICAM	quantitative filtration technique with an integrative-cavity absorption meter setup
1051	Xyl	xylose

## 1052 References

- 1053 Alderkamp, A.-C., Buma, A. G. J., and van Rijssel, M.: The carbohydrates of *Phaeocystis* and their degradation in the microbial  
1054 food web, *Biogeochemistry*, 83, 99–118, <https://doi.org/10.1007/s10533-007-9078-2>, 2007.
- 1055 Aller, J. Y., Kuznetsova, M. R., Jahns, C. J., and Kemp, P. F.: The sea surface microlayer as a source of viral and bacterial  
1056 enrichment in marine aerosols, *Journal of Aerosol Science*, 36, 801–812, <https://doi.org/10.1016/j.jaerosci.2004.10.012>,  
1057 2005.
- 1058 Aller, J. Y., Radway, J. C., Kilhau, W. P., Bothe, D. W., Wilson, T. W., Vaillancourt, R. D., Quinn, P. K., Coffman, D. J., Murray,  
1059 B. J., and Knopf, D. A.: Size-resolved characterization of the polysaccharidic and proteinaceous components of sea spray  
1060 aerosol, *Atmospheric Environment*, 154, 331–347, <https://doi.org/10.1016/j.atmosenv.2017.01.053>, 2017.
- 1061 Alpert, P. A., Kilhau, W. P., O'Brien, R. E., Moffet, R. C., Gilles, M. K., Wang, B., Laskin, A., Aller, J. Y., and Knopf, D. A.: Ice-  
1062 nucleating agents in sea spray aerosol identified and quantified with a holistic multimodal freezing model, *Science Advances*,  
1063 8, eabq6842, <https://doi.org/10.1126/sciadv.abq6842>, 2022.
- 1064 Álvarez, E., Losa, S. N., Bracher, A., Thoms, S., and Völker, C.: Phytoplankton Light Absorption Impacted by Photoprotective  
1065 Carotenoids in a Global Ocean Spectrally-Resolved Biogeochemistry Model, *Journal of Advances in Modeling Earth Systems*,  
1066 14, e2022MS003126, <https://doi.org/10.1029/2022MS003126>, 2022.
- 1067 Amon, R. M. W., Fitznar, H.-P., and Benner, R.: Linkages among the bioreactivity, chemical composition, and diagenetic state  
1068 of marine dissolved organic matter, *Limnology and Oceanography*, 46, 287–297, 2001.
- 1069 Angle, K., Grassian, V. H., and Ault, A. P.: The rapid acidification of sea spray aerosols, *Physics today*, 75,  
1070 <https://doi.org/10.1063/PT.3.4926>, 2022.
- 1071 Angle, K. J., Crocker, D. R., Simpson, R. M. C., Mayer, K. J., Garofalo, L. A., Moore, A. N., Garcia, S. L. M., Or, V. W., Srinivasan,  
1072 S., Farhan, M., Sauer, J. S., Lee, C., Pothier, M. A., Farmer, D. K., Martz, T. R., Bertram, T. H., Cappa, C. D., Prather, K. A., and  
1073 Grassian, V. H.: Acidity across the interface from the ocean surface to sea spray aerosol, *PNAS*, 118,  
1074 <https://doi.org/10.1073/pnas.2018397118>, 2021.
- 1075 Arnosti, C.: Substrate specificity in polysaccharide hydrolysis: Contrasts between bottom water and sediments, *Limnology  
1076 and Oceanography*, 45, 1112–1119, <https://doi.org/10.4319/lo.2000.45.5.1112>, 2000.
- 1077 Aslam, S. N., Michel, C., Niemi, A., and Underwood, G. J. C.: Patterns and drivers of carbohydrate budgets in ice algal  
1078 assemblages from first year Arctic sea ice, *Limnology and Oceanography*, 61, 919–937, <https://doi.org/10.1002/lno.10260>,  
1079 2016.
- 1080 Azetsu-Scott, K. and Passow, U.: Ascending marine particles: Significance of transparent exopolymer particles (TEP) in the  
1081 upper ocean, *Limnology and Oceanography*, 49, 741–748, <https://doi.org/10.4319/lo.2004.49.3.0741>, 2004.
- 1082 Barlow, R., Cummings, D., and Gibb, S.: Improved resolution of mono- and divinyl chlorophylls a and b and zeaxanthin and  
1083 lutein in phytoplankton extracts using reverse phase C-8 HPLC, *Marine Ecology Progress Series*, 161, 303–307,  
1084 <https://doi.org/10.3354/meps161303>, 1997.
- 1085 Barthel, S., Tegen, I., and Wolke, R.: Do new sea spray aerosol source functions improve the results of a regional aerosol  
1086 model?, *Atmospheric Environment*, 198, 265–278, <https://doi.org/10.1016/j.atmosenv.2018.10.016>, 2019.
- 1087 Bates, N. R., Garley, R., Frey, K. E., Shake, K. L., and Mathis, J. T.: Sea-ice melt CO<sub>2</sub>-carbonate chemistry in the western Arctic  
1088 Ocean: meltwater contributions to air-sea CO<sub>2</sub> gas exchange, mixed-layer properties and rates of net community production  
1089 under sea ice, *Biogeosciences*, 11, 6769–6789, <https://doi.org/10.5194/bg-11-6769-2014>, 2014.
- 1090 Becker, S., Tebben, J., Coffinet, S., Wiltshire, K., Iversen, M. H., Harder, T., Hinrichs, K.-U., and Hehemann, J.-H.: Laminarin is  
1091 a major molecule in the marine carbon cycle, *PNAS*, 117, 6599–6607, <https://doi.org/10.1073/pnas.1917001117>, 2020.
- 1092 Benner, R. and Kaiser, K.: Abundance of amino sugars and peptidoglycan in marine particulate and dissolved organic matter,  
1093 *Limnology and Oceanography*, 48, 118–128, <https://doi.org/10.4319/lo.2003.48.1.0118>, 2003.
- 1094 Bigg, E. K. and Leck, C.: The composition of fragments of bubbles bursting at the ocean surface, *Journal of Geophysical  
1095 Research: Atmospheres*, 113, <https://doi.org/10.1029/2007JD009078>, 2008.
- 1096 Bikerman, J. J.: *Foams*, Springer Science & Business Media, 344 pp., 2013.
- 1097 Bozem, H., Hoor, P., Kunkel, D., Köllner, F., Schneider, J., Herber, A., Schulz, H., Leaitch, W. R., Aliabadi, A. A., Willis, M. D.,  
1098 Burkart, J., and Abbatt, J. P. D.: Characterization of transport regimes and the polar dome during Arctic spring and summer  
1099 using in situ aircraft measurements, *Atmospheric Chemistry and Physics*, 19, 15049–15071, <https://doi.org/10.5194/acp-19-15049-2019>, 2019.
- 1101 Bricaud, A., Claustre, H., Ras, J., and Oubelkheir, K.: Natural variability of phytoplanktonic absorption in oceanic waters:  
1102 Influence of the size structure of algal populations, *Journal of Geophysical Research: Oceans*, 109,  
1103 <https://doi.org/10.1029/2004JC002419>, 2004.

- 1104 Burrows, S. M., Ogunro, O., Frossard, A., Russell, L. M., Rasch, P. J., and Elliott, S.: A Physically Based Framework for Modelling  
1105 the Organic Fractionation of Sea Spray Aerosol from Bubble Film Langmuir Equilibria, *Atmospheric Chemistry and Physics*,  
1106 14(24):13601–13629, <https://doi.org/10.5194/acp-14-13601-2014>, 2014.
- 1107 Burrows, S. M., Gobrogge, E., Fu, L., Link, K., Elliott, S. M., Wang, H., and Walker, R.: OCEANFILMS-2: Representing  
1108 coadsorption of saccharides in marine films and potential impacts on modeled marine aerosol chemistry, *Geophysical*  
1109 *Research Letters*, 43, 8306–8313, <https://doi.org/10.1002/2016GL069070>, 2016.
- 1110 Callaghan, A. H., Deane, G. B., Stokes, M. D., and Ward, B.: Observed variation in the decay time of oceanic whitecap foam,  
1111 *Journal of Geophysical Research: Oceans*, 117, <https://doi.org/10.1029/2012JC008147>, 2012.
- 1112 Casillo, A., Lanzetta, R., Parrilli, M., and Corsaro, M. M.: Exopolysaccharides from Marine and Marine Extremophilic Bacteria:  
1113 Structures, Properties, Ecological Roles and Applications, *Marine Drugs*, 16, 69, <https://doi.org/10.3390/md16020069>, 2018.
- 1114 Chen, Q., Mirrieles, J. A., Thanekar, S., Loeb, N. A., Kirpes, R. M., Upchurch, L. M., Barget, A. J., Lata, N. N., Raso, A. R. W.,  
1115 McNamara, S. M., China, S., Quinn, P. K., Ault, A. P., Kennedy, A., Shepson, P. B., Fuentes, J. D., and Pratt, K. A.: Atmospheric  
1116 particle abundance and sea salt aerosol observations in the springtime Arctic: a focus on blowing snow and leads,  
1117 *Atmospheric Chemistry and Physics*, 22, 15263–15285, <https://doi.org/10.5194/acp-22-15263-2022>, 2022.
- 1118 Chi, J. W., Li, W. J., Zhang, D. Z., Zhang, J. C., Lin, Y. T., Shen, X. J., Sun, J. Y., Chen, J. M., Zhang, X. Y., Zhang, Y. M., and Wang,  
1119 W. X.: Sea salt aerosols as a reactive surface for inorganic and organic acidic gases in the Arctic troposphere, *Atmospheric*  
1120 *Chemistry and Physics*, 15, 11341–11353, <https://doi.org/10.5194/acp-15-11341-2015>, 2015.
- 1121 Creamean, J. M., Barry, K., Hill, T. C. J., Hume, C., DeMott, P. J., Shupe, M. D., Dahlke, S., Willmes, S., Schmale, J., Beck, I.,  
1122 Hoppe, C. J. M., Fong, A., Chamberlain, E., Bowman, J., Scharien, R., and Persson, O.: Annual cycle observations of aerosols  
1123 capable of ice formation in central Arctic clouds, *Nat Commun*, 13, 3537, <https://doi.org/10.1038/s41467-022-31182-x>, 2022.
- 1124 Cunliffe, M., Engel, A., Frka, S., Gašparović, B., Guitart, C., Murrell, J. C., Salter, M., Stolle, C., Upstill-Goddard, R., and Wurl,  
1125 O.: Sea surface microlayers: A unified physicochemical and biological perspective of the air–ocean interface, *Progress in*  
1126 *Oceanography*, 109, 104–116, <https://doi.org/10.1016/j.pocean.2012.08.004>, 2013.
- 1127 Cunliffe, M. and Wurl, O.: Guide to best practices to study the ocean’s surface., *Marine Biological Association of the United*  
1128 *Kingdom for SCOR*, 2014.
- 1129 Delort, A.-M., Vaïtilingom, M., Amato, P., Sancelme, M., Parazols, M., Mailhot, G., Laj, P., and Deguillaume, L.: A short  
1130 overview of the microbial population in clouds: Potential roles in atmospheric chemistry and nucleation processes,  
1131 *Atmospheric Research*, 98, 249–260, <https://doi.org/10.1016/j.atmosres.2010.07.004>, 2010.
- 1132 DeMott, P. J., Hill, T. C. J., McCluskey, C. S., Prather, K. A., Collins, D. B., Sullivan, R. C., Ruppel, M. J., Mason, R. H., Irish, V. E.,  
1133 Lee, T., Hwang, C. Y., Rhee, T. S., Snider, J. R., McMeeking, G. R., Dhaniyala, S., Lewis, E. R., Wentzell, J. J. B., Abbatt, J., Lee,  
1134 C., Sultana, C. M., Ault, A. P., Axson, J. L., Martinez, M. D., Venero, I., Santos-Figueroa, G., Stokes, M. D., Deane, G. B., Mayol-  
1135 Bracero, O. L., Grassian, V. H., Bertram, T. H., Bertram, A. K., Moffett, B. F., and Franc, G. D.: Sea spray aerosol as a unique  
1136 source of ice nucleating particles, *PNAS*, 113, 5797–5803, <https://doi.org/10.1073/pnas.1514034112>, 2016.
- 1137 Demoz, B. B., Collett, J. L., and Daube, B. C.: On the Caltech Active Strand Cloudwater Collectors, *Atmospheric Research*, 41,  
1138 47–62, [https://doi.org/10.1016/0169-8095\(95\)00044-5](https://doi.org/10.1016/0169-8095(95)00044-5), 1996.
- 1139 Dominutti, P. A., Renard, P., Vaïtilingom, M., Bianco, A., Baray, J.-L., Borbon, A., Bourianne, T., Burnet, F., Colomb, A., Delort,  
1140 A.-M., Dufлот, V., Houdier, S., Jaffrezo, J.-L., Joly, M., Leremboure, M., Metzger, J.-M., Pichon, J.-M., Ribeiro, M., Rocco, M.,  
1141 Tulet, P., Vella, A., Leriche, M., and Deguillaume, L.: Insights into tropical cloud chemistry in Réunion (Indian Ocean): results  
1142 from the BIO-MAÏDO campaign, *Atmospheric Chemistry and Physics*, 22, 505–533, <https://doi.org/10.5194/acp-22-505-2022>,  
1143 2022.
- 1144 Engbrodt, R.: Biogeochemistry of dissolved carbohydrates in the Arctic, *Berichte zur Polar-und Meeresforschung (Reports on*  
1145 *Polar and Marine Research)*, 396, 106pp, 2001.
- 1146 Engel, A. and Händel, N.: A novel protocol for determining the concentration and composition of sugars in particulate and in  
1147 high molecular weight dissolved organic matter (HMW-DOM) in seawater, *Marine Chemistry*, 127, 180–191,  
1148 <https://doi.org/10.1016/j.marchem.2011.09.004>, 2011.
- 1149 Engel, A., Bange, H. W., Cunliffe, M., Burrows, S. M., Friedrichs, G., Galgani, L., Herrmann, H., Hertkorn, N., Johnson, M., Liss,  
1150 P. S., Quinn, P. K., Schartau, M., Soloviev, A., Stolle, C., Upstill-Goddard, R. C., van Pinxteren, M., and Zäncker, B.: The Ocean’s  
1151 Vital Skin: Toward an Integrated Understanding of the Sea Surface Microlayer, *Front. Mar. Sci.*, 4, 165,  
1152 <https://doi.org/10.3389/fmars.2017.00165>, 2017.
- 1153 Ervens, B. and Amato, P.: The global impact of bacterial processes on carbon mass, *Atmospheric Chemistry & Physics*, 20,  
1154 1777–1794, <https://doi.org/10.5194/acp-20-1777-2020>, 2020.
- 1155 Fabiano, M., Povero, P., and Danovaro, R.: Distribution and composition of particulate organic matter in the Ross Sea  
1156 (Antarctica), *Polar Biol*, 13, 525–533, <https://doi.org/10.1007/BF00236394>, 1993.



- 1157 Facchini, M. C., Rinaldi, M., Decesari, S., Carbone, C., Finessi, E., Mircea, M., Fuzzi, S., Ceburnis, D., Flanagan, R., Nilsson, E. D.,  
1158 Leeuw, G. de, Martino, M., Woeltjen, J., and O'Dowd, C. D.: Primary submicron marine aerosol dominated by insoluble organic  
1159 colloids and aggregates, *Geophysical Research Letters*, 35, <https://doi.org/10.1029/2008GL034210>, 2008.
- 1160 Galgani, L., Piontek, J., and Engel, A.: Biopolymers form a gelatinous microlayer at the air-sea interface when Arctic sea ice  
1161 melts, *Scientific Reports*, 6, 29465, <https://doi.org/10.1038/srep29465>, 2016.
- 1162 Gantt, B., Meskhidze, N., Facchini, M. C., Rinaldi, M., Ceburnis, D., and O'Dowd, C. D.: Wind speed dependent size-resolved  
1163 parameterization for the organic mass fraction of sea spray aerosol, *Atmospheric Chemistry and Physics*, 11, 8777–8790,  
1164 <https://doi.org/10.5194/acp-11-8777-2011>, 2011.
- 1165 Gao, Q., Leck, C., Rauschenberg, C., and Matrai, P. A.: On the chemical dynamics of extracellular polysaccharides in the high  
1166 Arctic surface microlayer, *Ocean Science*, 8, 401–418, 2012.
- 1167 Gilardoni, S., Massoli, P., Giulianelli, L., Rinaldi, M., Paglione, M., Pollini, F., Lanconelli, C., Poluzzi, V., Carbone, S., Hillamo, R.,  
1168 Russell, L. M., Facchini, M. C., and Fuzzi, S.: Fog scavenging of organic and inorganic aerosol in the Po Valley, *Atmospheric  
1169 Chemistry and Physics*, 14, 6967–6981, <https://doi.org/10.5194/acp-14-6967-2014>, 2014.
- 1170 Goldberg, S. J., Carlson, C. A., Brzezinski, M., Nelson, N. B., and Siegel, D. A.: Systematic removal of neutral sugars within  
1171 dissolved organic matter across ocean basins, *Geophysical Research Letters*, 38, <https://doi.org/10.1029/2011GL048620>,  
1172 2011.
- 1173 Gonçalves-Araujo, R., Stedmon, C. A., Heim, B., Dubinenkov, I., Kraberg, A., Moiseev, D., and Bracher, A.: From Fresh to Marine  
1174 Waters: Characterization and Fate of Dissolved Organic Matter in the Lena River Delta Region, Siberia, *Frontiers in Marine  
1175 Science*, 2, 2015.
- 1176 Gong, X., Zhang, J., Croft, B., Yang, X., Frey, M. M., Bergner, N., Chang, R. Y.-W., Creamean, J. M., Kuang, C., Martin, R. V.,  
1177 Ranjithkumar, A., Sedlacek, A. J., Uin, J., Willmes, S., Zawadowicz, M. A., Pierce, J. R., Shupe, M. D., Schmale, J., and Wang, J.:  
1178 Arctic warming by abundant fine sea salt aerosols from blowing snow, *Nat. Geosci.*, 16, 768–774,  
1179 <https://doi.org/10.1038/s41561-023-01254-8>, 2023.
- 1180 Grythe, H., Ström, J., Krejci, R., Quinn, P., and Stohl, A.: A review of sea-spray aerosol source functions using a large global set  
1181 of sea salt aerosol concentration measurements, *Atmospheric Chemistry and Physics*, 14, 1277–1297,  
1182 <https://doi.org/10.5194/acp-14-1277-2014>, 2014.
- 1183 Haddrell, A. E. and Thomas, R. J.: Aerobiology: Experimental Considerations, Observations, and Future Tools, *Appl. Environ.  
1184 Microbiol.*, 83, <https://doi.org/10.1128/AEM.00809-17>, 2017.
- 1185 Hansell, D. A.: Recalcitrant Dissolved Organic Carbon Fractions, *Annual Review of Marine Science*, 5, 421–445,  
1186 <https://doi.org/10.1146/annurev-marine-120710-100757>, 2013.
- 1187 Hara, K., Yamagata, S., Yamanouchi, T., Sato, K., Herber, A., Iwasaka, Y., Nagatani, M., and Nakata, H.: Mixing states of  
1188 individual aerosol particles in spring Arctic troposphere during ASTAR 2000 campaign, *Journal of Geophysical Research:  
1189 Atmospheres*, 108, <https://doi.org/10.1029/2002JD002513>, 2003.
- 1190 Hartmann, M., Gong, X., Kecorius, S., van Pinxteren, M., Vogl, T., Welti, A., Wex, H., Zeppenfeld, S., Herrmann, H.,  
1191 Wiedensohler, A., and Stratmann, F.: Terrestrial or marine – indications towards the origin of ice-nucleating particles during  
1192 melt season in the European Arctic up to 83.7°&thinsp;N, *Atmospheric Chemistry and Physics*, 21, 11613–11636,  
1193 <https://doi.org/10.5194/acp-21-11613-2021>, 2021.
- 1194 Hasencz, E., Jayarathne, T., Pendergraft, M. A., Santander, M. V., Mayer, K. J., Sauer, J., Lee, C., Gibson, W. S., Kruse, S. M.,  
1195 Malfatti, F., Prather, K. A., and Stone, E. A.: Marine bacteria affect saccharide enrichment in sea spray aerosol during a  
1196 phytoplankton bloom, *ACS Earth Space Chem.*, 4, 1638–1649, <https://doi.org/10.1021/acsearthspacechem.0c00167>, 2020.
- 1197 Hasencz, E. S., Kaluarachchi, C. P., Lee, H. D., Tivanski, A. V., and Stone, E. A.: Saccharide Transfer to Sea Spray Aerosol  
1198 Enhanced by Surface Activity, Calcium, and Protein Interactions, *ACS Earth Space Chem.*, 3, 2539–2548,  
1199 <https://doi.org/10.1021/acsearthspacechem.9b00197>, 2019.
- 1200 Held, A., Brooks, I. M., Leck, C., and Tjernström, M.: On the potential contribution of open lead particle emissions to the  
1201 central Arctic aerosol concentration, *Atmospheric Chemistry and Physics*, 11, 3093–3105, <https://doi.org/10.5194/acp-11-3093-2011>, 2011.
- 1203 Herrmann, H., Schaefer, T., Tilgner, A., Styler, S. A., Weller, C., Teich, M., and Otto, T.: Tropospheric Aqueous-Phase Chemistry:  
1204 Kinetics, Mechanisms, and Its Coupling to a Changing Gas Phase, *Chem. Rev.*, 115, 4259–4334,  
1205 <https://doi.org/10.1021/cr500447k>, 2015.
- 1206 Hoffman, E. J. and Duce, R. A.: Factors influencing the organic carbon content of marine aerosols: A laboratory study, *Journal  
1207 of Geophysical Research (1896-1977)*, 81, 3667–3670, <https://doi.org/10.1029/JC081i021p03667>, 1976.
- 1208 Huang, J. and Jaeglé, L.: Wintertime enhancements of sea salt aerosol in polar regions consistent with a sea ice source from  
1209 blowing snow, *Atmos. Chem. Phys.*, 17, 3699–3712, <https://doi.org/10.5194/acp-17-3699-2017>, 2017.

- 1210 Istomina, L.: Retrieval of Sea Ice Surface Melt Using OLCI Data Onboard Sentinel-3, 2020, C017-07, 2020.
- 1211 Ittekkot, V., Brockmann, U., Michaelis, W., and Degens, E. T.: Dissolved free and combined carbohydrates during a  
1212 phytoplankton bloom in the northern North Sea, *Marine Ecology Progress Series*, 4, 299–305, 1981.
- 1213 Karl, M., Leck, C., Rad, F. M., Bäcklund, A., Lopez-Aparicio, S., and Heintzenberg, J.: New insights in sources of the sub-  
1214 micrometre aerosol at Mt. Zeppelin observatory (Spitsbergen) in the year 2015, *Tellus B: Chemical and Physical Meteorology*,  
1215 71, 1613143, <https://doi.org/10.1080/16000889.2019.1613143>, 2019.
- 1216 Kecorius, S., Vogl, T., Paasonen, P., Lampilahti, J., Rothenberg, D., Wex, H., Zeppenfeld, S., van Pinxteren, M., Hartmann, M.,  
1217 Henning, S., Gong, X., Welti, A., Kulmala, M., Stratmann, F., Herrmann, H., and Wiedensohler, A.: New particle formation and  
1218 its effect on cloud condensation nuclei abundance in the summer Arctic: a case study in the Fram Strait and Barents Sea,  
1219 *Atmospheric Chemistry and Physics*, 19, 14339–14364, <https://doi.org/10.5194/acp-19-14339-2019>, 2019.
- 1220 Keene, W. C., Long, M. S., Reid, J. S., Frossard, A. A., Kieber, D. J., Maben, J. R., Russell, L. M., Kinsey, J. D., Quinn, P. K., and  
1221 Bates, T. S.: Factors That Modulate Properties of Primary Marine Aerosol Generated From Ambient Seawater on Ships at Sea,  
1222 *Journal of Geophysical Research: Atmospheres*, 122, 11,961–11,990, <https://doi.org/10.1002/2017JD026872>, 2017.
- 1223 Kirchman, D. L., Meon, B., Ducklow, H. W., Carlson, C. A., Hansell, D. A., and Steward, G. F.: Glucose fluxes and concentrations  
1224 of dissolved combined neutral sugars (polysaccharides) in the Ross Sea and Polar Front Zone, Antarctica, *Deep Sea Research*  
1225 *Part II: Topical Studies in Oceanography*, 48, 4179–4197, [https://doi.org/10.1016/S0967-0645\(01\)00085-6](https://doi.org/10.1016/S0967-0645(01)00085-6), 2001.
- 1226 Kirpes, R. M., Bondy, A. L., Bonanno, D., Moffet, R. C., Wang, B., Laskin, A., Ault, A. P., and Pratt, K. A.: Secondary sulfate is  
1227 internally mixed with sea spray aerosol and organic aerosol in the winter Arctic, *Atmos. Chem. Phys.*, 18, 3937–3949,  
1228 <https://doi.org/10.5194/acp-18-3937-2018>, 2018.
- 1229 Krembs, C. and Deming, J. W.: The role of exopolymers in microbial adaptation to sea ice, in: *Psychrophiles: from biodiversity*  
1230 *to biotechnology*, Springer, 247–264, 2008.
- 1231 Krembs, C., Eicken, H., Junge, K., and Deming, J. W.: High concentrations of exopolymeric substances in Arctic winter sea ice:  
1232 implications for the polar ocean carbon cycle and cryoprotection of diatoms, *Deep Sea Research Part I: Oceanographic*  
1233 *Research Papers*, 49, 2163–2181, [https://doi.org/10.1016/S0967-0637\(02\)00122-X](https://doi.org/10.1016/S0967-0637(02)00122-X), 2002.
- 1234 Kubota, H., Ogiwara, Y., and Matsuzaki, K.: Photo-Induced Formation of Peroxide in Saccharides and Related Compounds,  
1235 *Polymer Journal*, 8, 557–563, <https://doi.org/10.1295/polymj.8.557>, 1976.
- 1236 Kumai, M.: Arctic Fog Droplet Size Distribution and Its Effect on Light Attenuation, *Journal of the Atmospheric Sciences*, 30,  
1237 635–643, [https://doi.org/10.1175/1520-0469\(1973\)030<0635:AFDSDA>2.0.CO;2](https://doi.org/10.1175/1520-0469(1973)030<0635:AFDSDA>2.0.CO;2), 1973.
- 1238 Lawler, M. J., Saltzman, E. S., Karlsson, L., Zieger, P., Salter, M., Baccharini, A., Schmale, J., and Leck, C.: New Insights Into the  
1239 Composition and Origins of Ultrafine Aerosol in the Summertime High Arctic, *Geophysical Research Letters*, 48,  
1240 e2021GL094395, <https://doi.org/10.1029/2021GL094395>, 2021.
- 1241 Leck, C.: Chemical composition and sources of the high Arctic aerosol relevant for cloud formation, *Journal of Geophysical*  
1242 *Research*, 107, <https://doi.org/10.1029/2001JD001463>, 2002.
- 1243 Leck, C., Gao, Q., Mashayekhy Rad, F., and Nilsson, U.: Size-resolved atmospheric particulate polysaccharides in the high  
1244 summer Arctic, *Atmospheric Chemistry and Physics*, 13, 12573–12588, <https://doi.org/10.5194/acp-13-12573-2013>, 2013.
- 1245 Lefering, I., Röttgers, R., Utschig, C., and McKee, D.: Uncertainty budgets for liquid waveguide CDOM absorption  
1246 measurements, *Appl. Opt.*, AO, 56, 6357–6366, <https://doi.org/10.1364/AO.56.006357>, 2017.
- 1247 Liu, Y., Röttgers, R., Ramírez-Pérez, M., Dinter, T., Steinmetz, F., Nöthig, E.-M., Hellmann, S., Wiegmann, S., and Bracher, A.:  
1248 Underway spectrophotometry in the Fram Strait (European Arctic Ocean): a highly resolved chlorophyll a data source for  
1249 complementing satellite ocean color, *Opt. Express*, OE, 26, A678–A696, <https://doi.org/10.1364/OE.26.00A678>, 2018.
- 1250 Macke, A. and Flores, H.: The Expeditions PS106/1 and 2 of the Research Vessel POLARSTERN to the Arctic Ocean in 2017,  
1251 Bremerhaven, Germany, 171 pp., [https://doi.org/10.2312/BzPM\\_0719\\_2018](https://doi.org/10.2312/BzPM_0719_2018), 2018.
- 1252 Malfatti, F., Lee, C., Tinta, T., Pendergraft, M. A., Celussi, M., Zhou, Y., Sultana, C. M., Rotter, A., Axson, J. L., Collins, D. B.,  
1253 Santander, M. V., Anides Morales, A. L., Aluwihare, L. I., Riemer, N., Grassian, V. H., Azam, F., and Prather, K. A.: Detection of  
1254 Active Microbial Enzymes in Nascent Sea Spray Aerosol: Implications for Atmospheric Chemistry and Climate, *Environ. Sci.*  
1255 *Technol. Lett.*, 6, 171–177, <https://doi.org/10.1021/acs.estlett.8b00699>, 2019.
- 1256 Mari, X., Passow, U., Migon, C., Burd, A. B., and Legendre, L.: Transparent exopolymer particles: Effects on carbon cycling in  
1257 the ocean, *Progress in Oceanography*, 151, 13–37, <https://doi.org/10.1016/j.pocean.2016.11.002>, 2017.
- 1258 Marks, R., Kruczalac, K., Jankowska, K., and Michalska, M.: Bacteria and fungi in air over the Gulf of Gdańsk and Baltic sea,  
1259 *Journal of Aerosol Science*, 32, 237–250, [https://doi.org/10.1016/S0021-8502\(00\)00064-1](https://doi.org/10.1016/S0021-8502(00)00064-1), 2001.
- 1260 Matsuoka, A., Bricaud, A., Benner, R., Para, J., Sempéré, R., Prieur, L., Bélanger, S., and Babin, M.: Tracing the transport of  
1261 colored dissolved organic matter in water masses of the Southern Beaufort Sea: relationship with hydrographic  
1262 characteristics, *Biogeosciences*, 9, 925–940, <https://doi.org/10.5194/bg-9-925-2012>, 2012.

- 1263 Matsuoka, A., Hooker, S. B., Bricaud, A., Gentili, B., and Babin, M.: Estimating absorption coefficients of colored dissolved  
1264 organic matter (CDOM) using a semi-analytical algorithm for southern Beaufort Sea waters: application to deriving  
1265 concentrations of dissolved organic carbon from space, *Biogeosciences*, 10, 917–927, [https://doi.org/10.5194/bg-10-917-](https://doi.org/10.5194/bg-10-917-2013)  
1266 2013, 2013.
- 1267 Matulová, M., Husárová, S., Capek, P., Sancelme, M., and Delort, A.-M.: Biotransformation of Various Saccharides and  
1268 Production of Exopolymeric Substances by Cloud-Borne *Bacillus* sp. 3B6, *Environ. Sci. Technol.*, 48, 14238–14247,  
1269 <https://doi.org/10.1021/es501350s>, 2014.
- 1270 May, N. W., Quinn, P. K., McNamara, S. M., and Pratt, K. A.: Multiyear study of the dependence of sea salt aerosol on wind  
1271 speed and sea ice conditions in the coastal Arctic: ARCTIC SEA SALT AEROSOL, *J. Geophys. Res. Atmos.*, 121, 9208–9219,  
1272 <https://doi.org/10.1002/2016JD025273>, 2016.
- 1273 Mayol, E., Arrieta, J. M., Jiménez, M. A., Martínez-Asensio, A., Garcias-Bonet, N., Dachs, J., González-Gaya, B., Royer, S.-J.,  
1274 Benítez-Barrios, V. M., Fraile-Nuez, E., and Duarte, C. M.: Long-range transport of airborne microbes over the global tropical  
1275 and subtropical ocean, *Nature Communications*, 8, 1–9, <https://doi.org/10.1038/s41467-017-00110-9>, 2017.
- 1276 McCarthy, M., Hedges, J., and Benner, R.: Major biochemical composition of dissolved high molecular weight organic matter  
1277 in seawater, *Marine Chemistry*, 55, 281–297, [https://doi.org/10.1016/S0304-4203\(96\)00041-2](https://doi.org/10.1016/S0304-4203(96)00041-2), 1996.
- 1278 McCluskey, C. S., Hill, T. C. J., Humphries, R. S., Rauker, A. M., Moreau, S., Strutton, P. G., Chambers, S. D., Williams, A. G.,  
1279 McRobert, I., Ward, J., Keywood, M. D., Harnwell, J., Ponsonby, W., Loh, Z. M., Krummel, P. B., Protat, A., Kreidenweis, S. M.,  
1280 and DeMott, P. J.: Observations of Ice Nucleating Particles Over Southern Ocean Waters, *Geophysical Research Letters*, 45,  
1281 11,989–11,997, <https://doi.org/10.1029/2018GL079981>, 2018.
- 1282 Mimura, T. and Romano, J. C.: Muramic Acid measurements for bacterial investigations in marine environments by high-  
1283 pressure liquid chromatography, *Appl. Environ. Microbiol.*, 50, 229–237, <https://doi.org/10.1128/AEM.50.2.229-237.1985>,  
1284 1985.
- 1285 Mühlenbruch, M., Grossart, H.-P., Eigemann, F., and Voss, M.: Mini-review: Phytoplankton-derived polysaccharides in the  
1286 marine environment and their interactions with heterotrophic bacteria, *Environmental Microbiology*, 20, 2671–2685,  
1287 <https://doi.org/10.1111/1462-2920.14302>, 2018.
- 1288 Müller, K., Lehmann, S., Pinxteren, D. van, Gnauk, T., Niedermeier, N., Wiedensohler, A., and Herrmann, H.: Particle  
1289 characterization at the Cape Verde atmospheric observatory during the 2007 RHaMBLe intensive, *Atmospheric Chemistry  
1290 and Physics*, 10, 2709–2721, <https://doi.org/10.5194/acp-10-2709-2010>, 2010.
- 1291 Norris, S. J., Brooks, I. M., de Leeuw, G., Sirevaag, A., Leck, C., Brooks, B. J., Birch, C. E., and Tjernström, M.: Measurements of  
1292 bubble size spectra within leads in the Arctic summer pack ice, *Ocean Science*, 7, 129–139, [https://doi.org/10.5194/os-7-129-](https://doi.org/10.5194/os-7-129-2011)  
1293 2011, 2011.
- 1294 Notz, D. and Worster, M. G.: Desalination processes of sea ice revisited, *Journal of Geophysical Research: Oceans*, 114,  
1295 <https://doi.org/10.1029/2008JC004885>, 2009.
- 1296 Obernosterer, I., Catala, P., Lami, R., Caparros, J., Ras, J., Bricaud, A., Christine, D., Van Wambeke, F., and Lebaron, P.:  
1297 Biochemical characteristics and bacterial community structure of the sea surface microlayer in the South Pacific Ocean,  
1298 *Biogeosciences*, 5, 693–705, 2008.
- 1299 O’Dowd, C. D., Facchini, M. C., Cavalli, F., Ceburnis, D., Mircea, M., Decesari, S., Fuzzi, S., Yoon, Y. J., and Putaud, J.-P.:  
1300 Biogenically driven organic contribution to marine aerosol, *Nature*, 431, 676–680, <https://doi.org/10.1038/nature02959>,  
1301 2004.
- 1302 Orellana, M. V., Matrai, P. A., Leck, C., Rauschenberg, C. D., Lee, A. M., and Coz, E.: Marine microgels as a source of cloud  
1303 condensation nuclei in the high Arctic, *PNAS*, 108, 13612–13617, <https://doi.org/10.1073/pnas.1102457108>, 2011.
- 1304 Panagiotopoulos, C. and Sempéré, R.: Analytical methods for the determination of sugars in marine samples: A historical  
1305 perspective and future directions, *Limnology and Oceanography: Methods*, 3, 419–454,  
1306 <https://doi.org/10.4319/lom.2005.3.419>, 2005.
- 1307 Papakonstantinou-Presvelou, I., Sourdeval, O., and Quaas, J.: Strong Ocean/Sea-Ice Contrasts Observed in Satellite-Derived  
1308 Ice Crystal Number Concentrations in Arctic Ice Boundary-Layer Clouds, *Geophysical Research Letters*, 49, e2022GL098207,  
1309 <https://doi.org/10.1029/2022GL098207>, 2022.
- 1310 Passow, U.: Transparent exopolymer particles (TEP) in aquatic environments, *Progress in Oceanography*, 55, 287–333,  
1311 [https://doi.org/10.1016/S0079-6611\(02\)00138-6](https://doi.org/10.1016/S0079-6611(02)00138-6), 2002.
- 1312 Penner, J. E., Andreae, M. O., Annegarn, H., Barrie, L., Feichter, J., Hegg, D., Jayaraman, A., Leitch, R., Murphy, D., Nganga,  
1313 J., and Pitari, G.: Aerosols, their Direct and Indirect Effects, *Climate Change 2001: The Scientific Basis. Contribution of Working  
1314 Group I to the Third Assessment Report of the Intergovernmental Panel on Climate Change*, 289–348, 2001.
- 1315 Phongphattarawat, S.: Variability in pigment composition and bio-optical characteristics of phytoplankton populations in the  
1316 Atlantic basin, <http://purl.org/dc/dcmitype/Text>, University of Oxford, 2016.

- 1317 van Pinxteren, M., Müller, C., Iinuma, Y., Stolle, C., and Herrmann, H.: Chemical Characterization of Dissolved Organic  
1318 Compounds from Coastal Sea Surface Microlayers (Baltic Sea, Germany), *Environmental Science & Technology*, 46, 10455–  
1319 10462, <https://doi.org/10.1021/es204492b>, 2012.
- 1320 van Pinxteren, M., Barthel, S., Fomba, K. W., Müller, K., Von Tümpling, W., and Herrmann, H.: The influence of environmental  
1321 drivers on the enrichment of organic carbon in the sea surface microlayer and in submicron aerosol particles – measurements  
1322 from the Atlantic Ocean, *Elem Sci Anth*, 5, <https://doi.org/10.1525/elementa.225>, 2017.
- 1323 van Pinxteren, M., Robinson, T.-B., Zeppenfeld, S., Gong, X., Bahlmann, E., Fomba, K. W., Triesch, N., Stratmann, F., Wurl, O.,  
1324 Engel, A., Wex, H., and Herrmann, H.: High number concentrations of transparent exopolymer particles in ambient aerosol  
1325 particles and cloud water – a case study at the tropical Atlantic Ocean, *Atmospheric Chemistry and Physics*, 22, 5725–5742,  
1326 <https://doi.org/10.5194/acp-22-5725-2022>, 2022.
- 1327 van Pinxteren, M., Zeppenfeld, S., Fomba, K. W., Triesch, N., Frka, S., and Herrmann, H.: Amino acids, carbohydrates, and  
1328 lipids in the tropical oligotrophic Atlantic Ocean: sea-to-air transfer and atmospheric in situ formation, *Atmospheric Chemistry  
1329 and Physics*, 23, 6571–6590, <https://doi.org/10.5194/acp-23-6571-2023>, 2023.
- 1330 Piontek, J., Lunau, M., Händel, N., Borchard, C., Wurst, M., and Engel, A.: Acidification increases microbial polysaccharide  
1331 degradation in the ocean, *Biogeosciences*, 7, 1615–1624, <https://doi.org/10.5194/bg-7-1615-2010>, 2010.
- 1332 Porter, G. C. E., Adams, M. P., Brooks, I. M., Ickes, L., Karlsson, L., Leck, C., Salter, M. E., Schmale, J., Siegel, K., Sikora, S. N. F.,  
1333 Tarn, M. D., Vüllers, J., Wernli, H., Zieger, P., Zinke, J., and Murray, B. J.: Highly Active Ice-Nucleating Particles at the Summer  
1334 North Pole, *Journal of Geophysical Research: Atmospheres*, 127, e2021JD036059, <https://doi.org/10.1029/2021JD036059>,  
1335 2022.
- 1336 Prather, K. A., Bertram, T. H., Grassian, V. H., Deane, G. B., Stokes, M. D., DeMott, P. J., Aluwihare, L. I., Palenik, B. P., Azam,  
1337 F., Seinfeld, J. H., Moffet, R. C., Molina, M. J., Cappa, C. D., Geiger, F. M., Roberts, G. C., Russell, L. M., Ault, A. P., Baltrusaitis,  
1338 J., Collins, D. B., Corrigan, C. E., Cuadra-Rodriguez, L. A., Ebben, C. J., Forestieri, S. D., Guasco, T. L., Hersey, S. P., Kim, M. J.,  
1339 Lambert, W. F., Modini, R. L., Mui, W., Pedler, B. E., Ruppel, M. J., Ryder, O. S., Schoepp, N. G., Sullivan, R. C., and Zhao, D.:  
1340 Bringing the ocean into the laboratory to probe the chemical complexity of sea spray aerosol, *PNAS*, 110, 7550–7555,  
1341 <https://doi.org/10.1073/pnas.1300262110>, 2013.
- 1342 Qin, G., Zhu, L., Chen, X., Wang, P. G., and Zhang, Y.: Structural characterization and ecological roles of a novel  
1343 exopolysaccharide from the deep-sea psychrotolerant bacterium *Pseudoalteromonas* sp. SM9913, *Microbiology*, 153, 1566–  
1344 1572, <https://doi.org/10.1099/mic.0.2006/003327-0>, 2007.
- 1345 Quinn, P. K., Collins, D. B., Grassian, V. H., Prather, K. A., and Bates, T. S.: Chemistry and Related Properties of Freshly Emitted  
1346 Sea Spray Aerosol, *Chemical Reviews*, 115, 4383–4399, <https://doi.org/10.1021/cr500713g>, 2015.
- 1347 Rastelli, E., Corinaldesi, C., Dell’Anno, A., Lo Martire, M., Greco, S., Cristina Facchini, M., Rinaldi, M., O’Dowd, C., Ceburnis, D.,  
1348 and Danovaro, R.: Transfer of labile organic matter and microbes from the ocean surface to the marine aerosol: an  
1349 experimental approach, *Scientific Reports*, 7, 1–10, <https://doi.org/10.1038/s41598-017-10563-z>, 2017.
- 1350 Rérolle, V., Ruiz-Pino, D., Rafizadeh, M., Loucaides, S., Papadimitriou, S., Mowlem, M., and Chen, J.: Measuring pH in the  
1351 Arctic Ocean: Colorimetric method or SeaFET?, *Methods in Oceanography*, 17, 32–49,  
1352 <https://doi.org/10.1016/j.mio.2016.05.006>, 2016.
- 1353 Robinson, T.-B., Wurl, O., Bahlmann, E., Jürgens, K., and Stolle, C.: Rising bubbles enhance the gelatinous nature of the air–  
1354 sea interface, *Limnology and Oceanography*, 64, 2358–2372, <https://doi.org/10.1002/lno.11188>, 2019.
- 1355 Rolph, R. J., Feltham, D. L., and Schröder, D.: Changes of the Arctic marginal ice zone during the satellite era, *The Cryosphere*,  
1356 14, 1971–1984, <https://doi.org/10.5194/tc-14-1971-2020>, 2020.
- 1357 Röttgers, R., McKee, D., and Utschig, C.: Temperature and salinity correction coefficients for light absorption by water in the  
1358 visible to infrared spectral region, *Opt. Express*, OE, 22, 25093–25108, <https://doi.org/10.1364/OE.22.025093>, 2014.
- 1359 Röttgers, R., Doxaran, D., and Dupouy, C.: Quantitative filter technique measurements of spectral light absorption by aquatic  
1360 particles using a portable integrating cavity absorption meter (QFT-ICAM), *Opt. Express*, OE, 24, A1–A20,  
1361 <https://doi.org/10.1364/OE.24.0000A1>, 2016.
- 1362 Russell, L. M., Hawkins, L. N., Frossard, A. A., Quinn, P. K., and Bates, T. S.: Carbohydrate-like composition of submicron  
1363 atmospheric particles and their production from ocean bubble bursting, *Proc. Natl. Acad. Sci. U.S.A.*, 107, 6652–6657,  
1364 <https://doi.org/10.1073/pnas.0908905107>, 2010.
- 1365 Šantl-Temkiv, T., Gosewinkel, U., Starnawski, P., Lever, M., and Finster, K.: Aeolian dispersal of bacteria in southwest  
1366 Greenland: their sources, abundance, diversity and physiological states, *FEMS Microbiol Ecol*, 94,  
1367 <https://doi.org/10.1093/femsec/fiy031>, 2018.
- 1368 Šantl-Temkiv, T., Sikoparija, B., Maki, T., Carotenuto, F., Amato, P., Yao, M., Morris, C. E., Schnell, R., Jaenicke, R., Pöhlker, C.,  
1369 DeMott, P. J., Hill, T. C. J., and Huffman, J. A.: Bioaerosol field measurements: Challenges and perspectives in outdoor studies,  
1370 *Aerosol Science and Technology*, 54, 520–546, <https://doi.org/10.1080/02786826.2019.1676395>, 2020.

- 1371 Schiffer, J. M., Mael, L. E., Prather, K. A., Amaro, R. E., and Grassian, V. H.: Sea Spray Aerosol: Where Marine Biology Meets  
1372 Atmospheric Chemistry, *ACS Cent. Sci.*, 4, 1617–1623, <https://doi.org/10.1021/acscentsci.8b00674>, 2018.
- 1373 Schill, S. R., Burrows, S. M., Hasenecz, E. S., Stone, E. A., and Bertram, T. H.: The Impact of Divalent Cations on the Enrichment  
1374 of Soluble Saccharides in Primary Sea Spray Aerosol, *Atmosphere*, 9, 476, <https://doi.org/10.3390/atmos9120476>, 2018.
- 1375 Schmale, J., Zieger, P., and Ekman, A. M. L.: Aerosols in current and future Arctic climate, *Nature Climate Change*, 11, 95–105,  
1376 <https://doi.org/10.1038/s41558-020-00969-5>, 2021.
- 1377 Schmithüsen, H.: Continuous meteorological surface measurement during POLARSTERN cruise PS106/1 (ARK-XXXI/1.1),  
1378 <https://doi.org/10.1594/PANGAEA.886302>, 2018.
- 1379 Schmithüsen, H.: Continuous meteorological surface measurement during POLARSTERN cruise PS106/2 (ARK-XXXI/1.2),  
1380 <https://doi.org/10.1594/PANGAEA.901179>, 2019.
- 1381 Schmitt-Kopplin, P., Liger-Belair, G., Koch, B. P., Flerus, R., Kattner, G., Harir, M., Kanawati, B., Lucio, M., Tziotis, D., Hertkorn,  
1382 N., and Gebefügi, I.: Dissolved organic matter in sea spray: a transfer study from marine surface water to aerosols,  
1383 *Biogeosciences*, 9, 1571–1582, 2012.
- 1384 Sellegri, K., O’Dowd, C. D., Yoon, Y. J., Jennings, S. G., and Leeuw, G. de: Surfactants and submicron sea spray generation,  
1385 *Journal of Geophysical Research: Atmospheres*, 111, <https://doi.org/10.1029/2005JD006658>, 2006.
- 1386 Spencer, R. G. M., Aiken, G. R., Butler, K. D., Dornblaser, M. M., Striegl, R. G., and Hernes, P. J.: Utilizing chromophoric dissolved  
1387 organic matter measurements to derive export and reactivity of dissolved organic carbon exported to the Arctic Ocean: A  
1388 case study of the Yukon River, Alaska, *Geophysical Research Letters*, 36, <https://doi.org/10.1029/2008GL036831>, 2009.
- 1389 Stedmon, C. A., Amon, R. M. W., Rinehart, A. J., and Walker, S. A.: The supply and characteristics of colored dissolved organic  
1390 matter (CDOM) in the Arctic Ocean: Pan Arctic trends and differences, *Marine Chemistry*, 124, 108–118,  
1391 <https://doi.org/10.1016/j.marchem.2010.12.007>, 2011.
- 1392 Stein, A. F., Draxler, R. R., Rolph, G. D., Stunder, B. J. B., Cohen, M. D., and Ngan, F.: NOAA’s HYSPLIT Atmospheric Transport  
1393 and Dispersion Modeling System, *Bull. Amer. Meteor. Soc.*, 96, 2059–2077, <https://doi.org/10.1175/BAMS-D-14-00110.1>,  
1394 2015.
- 1395 Stolle, C., Nagel, K., Labrenz, M., and Jürgens, K.: Succession of the sea-surface microlayer in the coastal Baltic Sea under  
1396 natural and experimentally induced low-wind conditions, *Biogeosciences*, 7, 2975–2988, [https://doi.org/10.5194/bg-7-2975-](https://doi.org/10.5194/bg-7-2975-2010)  
1397 2010, 2010.
- 1398 Strong, C. and Rigor, I. G.: Arctic marginal ice zone trending wider in summer and narrower in winter, *Geophysical Research*  
1399 *Letters*, 40, 4864–4868, <https://doi.org/10.1002/grl.50928>, 2013.
- 1400 Sud, I. J. and Tyler, M. E.: Cell-Wall Composition and Osmotic Fragility of Selected Marine Bacteria, *Journal of Bacteriology*,  
1401 87, 696–700, 1964.
- 1402 Suzuki, E. and Suzuki, R.: Variation of Storage Polysaccharides in Phototrophic Microorganisms, *Journal of Applied*  
1403 *Glycoscience*, 60, 21–27, [https://doi.org/10.5458/jag.jag.JAG-2012\\_016](https://doi.org/10.5458/jag.jag.JAG-2012_016), 2013.
- 1404 Taylor, B. B., Torrecilla, E., Bernhardt, A., Taylor, M. H., Peeken, I., Röttgers, R., Piera, J., and Bracher, A.: Bio-optical provinces  
1405 in the eastern Atlantic Ocean and their biogeographical relevance, 8, 7165–7219, <https://doi.org/10.5194/bgd-8-7165-2011>,  
1406 2011.
- 1407 Thomson, J.: Wave propagation in the marginal ice zone: connections and feedback mechanisms within the air–ice–ocean  
1408 system, *Philosophical Transactions of the Royal Society A: Mathematical, Physical and Engineering Sciences*, 380, 20210251,  
1409 <https://doi.org/10.1098/rsta.2021.0251>, 2022.
- 1410 Triesch, N., van Pinxteren, M., Engel, A., and Herrmann, H.: Concerted measurements of free amino acids at the Cabo Verde  
1411 islands: high enrichments in submicron sea spray aerosol particles and cloud droplets, *Atmospheric Chemistry and Physics*,  
1412 21, 163–181, <https://doi.org/10.5194/acp-21-163-2021>, 2021a.
- 1413 Triesch, N., van Pinxteren, M., Frka, S., Stolle, C., Spranger, T., Hoffmann, E. H., Gong, X., Wex, H., Schulz-Bull, D., Gašparović,  
1414 B., and Herrmann, H.: Concerted measurements of lipids in seawater and on submicrometer aerosol particles at the Cabo  
1415 Verde islands: biogenic sources, selective transfer and high enrichments, *Atmospheric Chemistry and Physics*, 21, 4267–4283,  
1416 <https://doi.org/10.5194/acp-21-4267-2021>, 2021b.
- 1417 Triesch, N., van Pinxteren, M., Salter, M., Stolle, C., Pereira, R., Zieger, P., and Herrmann, H.: Sea Spray Aerosol Chamber Study  
1418 on Selective Transfer and Enrichment of Free and Combined Amino Acids, *ACS Earth Space Chem.*, 5, 1564–1574,  
1419 <https://doi.org/10.1021/acsearthspacechem.1c00080>, 2021c.
- 1420 Trueblood, J. V., Wang, X., Or, V. W., Alves, M. R., Santander, M. V., Prather, K. A., and Grassian, V. H.: The Old and the New:  
1421 Aging of Sea Spray Aerosol and Formation of Secondary Marine Aerosol through OH Oxidation Reactions, *ACS Earth Space*  
1422 *Chem.*, 3, 2307–2314, <https://doi.org/10.1021/acsearthspacechem.9b00087>, 2019.

- 1423 Tynan, E., Clarke, J. S., Humphreys, M. P., Ribas-Ribas, M., Esposito, M., Rérolle, V. M. C., Schlosser, C., Thorpe, S. E., Tyrrell,  
1424 T., and Achterberg, E. P.: Physical and biogeochemical controls on the variability in surface pH and calcium carbonate  
1425 saturation states in the Atlantic sectors of the Arctic and Southern Oceans, *Deep Sea Research Part II: Topical Studies in*  
1426 *Oceanography*, 127, 7–27, <https://doi.org/10.1016/j.dsr2.2016.01.001>, 2016.
- 1427 Uetake, J., Hill, T. C. J., Moore, K. A., DeMott, P. J., Protat, A., and Kreidenweis, S. M.: Airborne bacteria confirm the pristine  
1428 nature of the Southern Ocean boundary layer, *PNAS*, 117, 13275–13282, <https://doi.org/10.1073/pnas.2000134117>, 2020.
- 1429 Vaqué, D., Boras, J. A., Arrieta, J. M., Agustí, S., Duarte, C. M., and Sala, M. M.: Enhanced Viral Activity in the Surface Microlayer  
1430 of the Arctic and Antarctic Oceans, *Microorganisms*, 9, 317, <https://doi.org/10.3390/microorganisms9020317>, 2021.
- 1431 Veron, F.: Ocean Spray, *Annual Review of Fluid Mechanics*, 47, 507–538, <https://doi.org/10.1146/annurev-fluid-010814-014651>, 2015.
- 1433 Walker, S. A., Amon, R. M. W., and Stedmon, C. A.: Variations in high-latitude riverine fluorescent dissolved organic matter:  
1434 A comparison of large Arctic rivers, *Journal of Geophysical Research: Biogeosciences*, 118, 1689–1702,  
1435 <https://doi.org/10.1002/2013JG002320>, 2013.
- 1436 Wang, X., Deane, G. B., Moore, K. A., Ryder, O. S., Stokes, M. D., Beall, C. M., Collins, D. B., Santander, M. V., Burrows, S. M.,  
1437 Sultana, C. M., and Prather, K. A.: The role of jet and film drops in controlling the mixing state of submicron sea spray aerosol  
1438 particles, *PNAS*, 114, 6978–6983, <https://doi.org/10.1073/pnas.1702420114>, 2017.
- 1439 Wendisch, M., Macke, A., Ehrlich, A., Lüpkes, C., Mech, M., Chechin, D., Dethloff, K., Barientos, C., Bozem, H., Brückner, M.,  
1440 Clemen, H.-C., Crewell, S., Donth, T., Dupuy, R., Ebell, K., Egerer, U., Engelmann, R., Engler, C., Eppers, O., Gehrman, M.,  
1441 Gong, X., Gottschalk, M., Goubeyre, C., Griesche, H., Hartmann, J., Hartmann, M., Heinold, B., Herber, A., Herrmann, H.,  
1442 Heygster, G., Hoor, P., Jafariserajehlou, S., Jäkel, E., Järvinen, E., Jourdan, O., Kästner, U., Kecorius, S., Knudsen, E. M., Köllner,  
1443 F., Kretzschmar, J., Lelli, L., Leroy, D., Maturilli, M., Mei, L., Mertes, S., Mioche, G., Neuber, R., Nicolaus, M., Nomokonova, T.,  
1444 Notholt, J., Palm, M., van Pinxteren, M., Quaas, J., Richter, P., Ruiz-Donoso, E., Schäfer, M., Schmieder, K., Schnaiter, M.,  
1445 Schneider, J., Schwarzenböck, A., Seifert, P., Shupe, M. D., Siebert, H., Spreen, G., Stapf, J., Stratmann, F., Vogl, T., Welti, A.,  
1446 Wex, H., Wiedensohler, A., Zanatta, M., and Zeppenfeld, S.: The Arctic Cloud Puzzle: Using ALOUD/PASCAL Multi-Platform  
1447 Observations to Unravel the Role of Clouds and Aerosol Particles in Arctic Amplification, *Bull. Amer. Meteor. Soc.*,  
1448 <https://doi.org/10.1175/BAMS-D-18-0072.1>, 2018.
- 1449 Wendisch, M., Brückner, M., Crewell, S., Ehrlich, A., Notholt, J., Lüpkes, C., Macke, A., Burrows, J. P., Rinke, A., Quaas, J.,  
1450 Maturilli, M., Schemann, V., Shupe, M. D., Akansu, E. F., Barrientos-Velasco, C., Bärfuss, K., Blechschmidt, A.-M., Block, K.,  
1451 Bougoudis, I., Bozem, H., Böckmann, C., Bracher, A., Bresson, H., Bretschneider, L., Buschmann, M., Chechin, D. G., Chylik, J.,  
1452 Dahlke, S., Deneke, H., Dethloff, K., Donth, T., Dorn, W., Dupuy, R., Ebell, K., Egerer, U., Engelmann, R., Eppers, O., Gerdes, R.,  
1453 Gierens, R., Gorodetskaya, I. V., Gottschalk, M., Griesche, H., Gryanik, V. M., Handorf, D., Harm-Altstädter, B., Hartmann, J.,  
1454 Hartmann, M., Heinold, B., Herber, A., Herrmann, H., Heygster, G., Höschel, I., Hofmann, Z., Hölemann, J., Hünnerbein, A.,  
1455 Jafariserajehlou, S., Jäkel, E., Jacobi, C., Janout, M., Jansen, F., Jourdan, O., Jurányi, Z., Kalesse-Los, H., Kanzow, T., Käthner,  
1456 R., Kliesch, L. L., Klingebiel, M., Knudsen, E. M., Kovács, T., Körtke, W., Krampe, D., Kretzschmar, J., Kreyling, D., Kulla, B.,  
1457 Kunkel, D., Lampert, A., Lauer, M., Lelli, L., Lerber, A. von Linke, O., Löhnert, U., Lonardi, M., Losa, S. N., Losch, M., Maahn,  
1458 M., Mech, M., Mei, L., Mertes, S., Metzner, E., Mewes, D., Michaelis, J., Mioche, G., Moser, M., Nakoudi, K., Neggers, R.,  
1459 Neuber, R., Nomokonova, T., Oelker, J., Papakonstantinou-Presvelou, I., et al.: Atmospheric and Surface Processes, and  
1460 Feedback Mechanisms Determining Arctic Amplification: A Review of First Results and Prospects of the (AC)3 Project, *Bulletin*  
1461 *of the American Meteorological Society*, 104, E208–E242, <https://doi.org/10.1175/BAMS-D-21-0218.1>, 2023.
- 1462 Wietz, M., Wemheuer, B., Simon, H., Giebel, H.-A., Seibt, M. A., Daniel, R., Brinkhoff, T., and Simon, M.: Bacterial community  
1463 dynamics during polysaccharide degradation at contrasting sites in the Southern and Atlantic Oceans, *Environ. Microbiol.*, 17,  
1464 3822–3831, <https://doi.org/10.1111/1462-2920.12842>, 2015.
- 1465 Wilbourn, E. K., Thornton, D. C. O., Ott, C., Graff, J., Quinn, P. K., Bates, T. S., Betha, R., Russell, L. M., Behrenfeld, M. J., and  
1466 Brooks, S. D.: Ice Nucleation by Marine Aerosols Over the North Atlantic Ocean in Late Spring, *Journal of Geophysical*  
1467 *Research: Atmospheres*, 125, e2019JD030913, <https://doi.org/10.1029/2019JD030913>, 2020.
- 1468 Williams, P. M., Carlucci, A. F., Henrichs, S. M., Van Vleet, E. S., Horrigan, S. G., Reid, F. M. H., and Robertson, K. J.: Chemical  
1469 and microbiological studies of sea-surface films in the Southern Gulf of California and off the West Coast of Baja California,  
1470 *Marine Chemistry*, 19, 17–98, [https://doi.org/10.1016/0304-4203\(86\)90033-2](https://doi.org/10.1016/0304-4203(86)90033-2), 1986.
- 1471 Wurl, O., Miller, L., Röttgers, R., and Vagle, S.: The distribution and fate of surface-active substances in the sea-surface  
1472 microlayer and water column, *Marine Chemistry*, 115, 1–9, <https://doi.org/10.1016/j.marchem.2009.04.007>, 2009.
- 1473 Wurl, O., Miller, L., and Vagle, S.: Production and fate of transparent exopolymer particles in the ocean, *Journal of Geophysical*  
1474 *Research: Oceans*, 116, <https://doi.org/10.1029/2011JC007342>, 2011.
- 1475 Xu, M., Tsona Tchinda, N., Li, J., and Du, L.: Insoluble lipid film mediates transfer of soluble saccharides from the sea to the  
1476 atmosphere: the role of hydrogen bonding, *Atmospheric Chemistry and Physics*, 23, 2235–2249, <https://doi.org/10.5194/acp-23-2235-2023>, 2023.

- 1478 Xu, W., Ovadnevaite, J., Fossum, K. N., Lin, C., Huang, R.-J., Ceburnis, D., and O'Dowd, C.: Sea spray as an obscured source for  
1479 marine cloud nuclei, *Nat. Geosci.*, 15, 282–286, <https://doi.org/10.1038/s41561-022-00917-2>, 2022.
- 1480 Yang, X., Pyle, J. A., and Cox, R. A.: Sea salt aerosol production and bromine release: Role of snow on sea ice, *Geophysical  
1481 Research Letters*, 35, <https://doi.org/10.1029/2008GL034536>, 2008.
- 1482 Zábory, J., Matisāns, M., Krejci, R., Nilsson, E. D., and Ström, J.: Artificial primary marine aerosol production: a laboratory study  
1483 with varying water temperature, salinity, and succinic acid concentration, *Atmospheric Chemistry and Physics*, 12, 10709–  
1484 10724, <https://doi.org/10.5194/acp-12-10709-2012>, 2012.
- 1485 Zäncker, B., Bracher, A., Röttgers, R., and Engel, A.: Variations of the Organic Matter Composition in the Sea Surface  
1486 Microlayer: A Comparison between Open Ocean, Coastal, and Upwelling Sites Off the Peruvian Coast, *Frontiers in  
1487 Microbiology*, 8, 2369, <https://doi.org/10.3389/fmicb.2017.02369>, 2017.
- 1488 Zäncker, B., Cunliffe, M., and Engel, A.: Eukaryotic community composition in the sea surface microlayer across an east–west  
1489 transect in the Mediterranean Sea, *Biogeosciences*, 18, 2107–2118, <https://doi.org/10.5194/bg-18-2107-2021>, 2021.
- 1490 Zeppenfeld, S., van Pinxteren, M., Hartmann, M., Bracher, A., Stratmann, F., and Herrmann, H.: Glucose as a Potential  
1491 Chemical Marker for Ice Nucleating Activity in Arctic Seawater and Melt Pond Samples, *Environ. Sci. Technol.*, 53, 8747–8756,  
1492 <https://doi.org/10.1021/acs.est.9b01469>, 2019a.
- 1493 Zeppenfeld, S., van Pinxteren, M., Hartmann, M., Bracher, A., Wiegmann, S., Stratmann, F., and Herrmann, H.: Glucose, T50  
1494 and salinity in the surface microlayer and bulk water samples from the Arctic during POLARSTERN cruise PS106 (2017),  
1495 <https://doi.org/10.1594/PANGAEA.899258>, 2019b.
- 1496 Zeppenfeld, S., van Pinxteren, M., Engel, A., and Herrmann, H.: A protocol for quantifying mono- and polysaccharides in  
1497 seawater and related saline matrices by electro-dialysis (ED) – combined with HPAEC-PAD, *Ocean Science*, 16, 817–830,  
1498 <https://doi.org/10.5194/os-16-817-2020>, 2020.
- 1499 Zeppenfeld, S., van Pinxteren, M., van Pinxteren, D., Wex, H., Berdalet, E., Vaqué, D., Dall'Osto, M., and Herrmann, H.: Aerosol  
1500 Marine Primary Carbohydrates and Atmospheric Transformation in the Western Antarctic Peninsula, *ACS Earth Space Chem.*,  
1501 5, 1032–1047, <https://doi.org/10.1021/acsearthspacechem.0c00351>, 2021a.
- 1502 Zeppenfeld, S., Fuchs, S., Rödger, S., Dietze, A., van Pinxteren, M., and Herrmann, H.: Marine carbohydrates and inorganic  
1503 ions in size-resolved atmospheric particles collected over the Southern Ocean, <https://doi.org/10.1594/PANGAEA.927565>,  
1504 2021b.
- 1505 Zeppenfeld, S., van Pinxteren, M., Fuchs, S., Hartmann, M., Gong, X., and Herrmann, H.: Inorganic ions in fog water sampled  
1506 from the Arctic in 2017, <https://doi.org/10.1594/PANGAEA.932573>, 2021c.
- 1507 Zeppenfeld, S., van Pinxteren, M., Fuchs, S., Hartmann, M., Gong, X., and Herrmann, H.: Inorganic ions in size-resolved aerosol  
1508 particles sampled from the Arctic in 2017, <https://doi.org/10.1594/PANGAEA.932569>, 2021d.
- 1509 Zeppenfeld, S., van Pinxteren, M., Fuchs, S., Hartmann, M., and Herrmann, H.: Combined carbohydrates, dissolved free  
1510 carbohydrates and pH in Arctic fog water sampled during PS106, <https://doi.org/10.1594/PANGAEA.962208>, 2023a.
- 1511 Zeppenfeld, S., van Pinxteren, M., Fuchs, S., Hartmann, M., and Herrmann, H.: Combined carbohydrates, organic carbon and  
1512 total aerosol mass concentrations in size-resolved aerosol particles sampled from the Arctic in 2017,  
1513 <https://doi.org/10.1594/PANGAEA.962210>, 2023b.
- 1514 Zeppenfeld, S., Bracher, A., Wiegmann, S., Zeising, M., Fuchs, S., van Pinxteren, M., and Herrmann, H.: Dissolved and  
1515 particulate combined carbohydrates, pH, inorganic ions, CDOM and particulate absorption of SML and bulk water in Arctic  
1516 surface seawater and melt ponds, <https://doi.org/10.1594/PANGAEA.961004>, 2023c.
- 1517 Zinke, J., Salter, M. E., Leck, C., Lawler, M. J., Porter, G. C. E., Adams, M. P., Brooks, I. M., Murray, B. J., and Zieger, P.: The  
1518 development of a miniaturised balloon-borne cloud water sampler and its first deployment in the high Arctic, *Tellus B:  
1519 Chemical and Physical Meteorology*, 73, 1–12, <https://doi.org/10.1080/16000889.2021.1915614>, 2021.